HOV

CONTROLLABILITY ANALYSIS USING FREQUENCY-DEPENDENT MEASURES FOR INTERACTIONS AND DISTURBANCES

Morten Hovd, Petter Lundström and Sigurd Skogestad *
Chemical Engineering
University of Trondheim, NTH
N-7034 Trondheim, Norway

November 9, 1990

Presented at AIChE Annual Meeting, Chicago, Nov. 11-16, 1990.

Abstract

By controllability (dynamic resilience) we generally mean the best closed-loop performance achievable using any controller. In this paper we limit us to linear single-loop (decentralized) controllers and study controllability in this case.

To evaluate controllability without actually having to design an optimal control system we need controller-independent measures. One such measure which has found widespread use is the relative gain array (RGA). We shall use as our main tools the frequency-dependent RGA, $\lambda_{ij}(s) = g_{ij}(s)[G^{-1}(s)]_{ji}$, and the Closed Loop Disturbance Gain (CLDG), $\delta_{ik}(s) = g_{ii}(s)[G(s)^{-1}G_d(s)]_{ik}$.

If $|\lambda|$ or $|\delta|$ are large at crossover frequencies then performance using single-loop controllers is expected to be poor. The values of δ_{ik} may tell the engineer which disturbance k will be most difficult to handle under feedback control. This may pinpoint the need for using feedforward control, or for modyfying the process by including, for example, a buffer tank for the feed. The paper is focused on applying these measures to distillation column control and fluid catalytic cracker (FCC) control.

*Author to whom correspondence should be addressed. E-mail: SKOGE@KJEMI.UNIT.NO, phone: 47-7-594154, fax: 47-7-591410

1 Introduction

The relative gain array (RGA) has found widespread use as a measure of interaction and as a tool for control structure selection for single-loop controllers. It was first introduced by Bristol (1966). It was originally defined at steady-state, but it may easily be extended to higher frequencies (Bristol, 1978). Shinskey (1967,1984) and several other authors have demonstrated practical applications of the RGA. Important advantages with the RGA is that it depends on the plant model only and that it is scaling independent. The advent of the computer has largely removed the need to develop simlified tools in order to save computation time. However, there are still a need for simple tools to yield insight and to assist the engineer in prescreening the large number of alternative control structures, and to get initial estimates of a systems achievable performance. The RGA is an ideal tool in this respect; it may be computed using only limited information and one calculation is sufficient for screening a large number of alternatives. However, there are of course limitations with such a simple tool, and more powerful and exact methods must be used after the initial screening.

For a 2×2 plant $G(s)$ the RGA-matrix is

$$\Lambda(s) = \begin{pmatrix} \lambda_{11} & \lambda_{12} \\ \lambda_{21} & \lambda_{22} \end{pmatrix} = \begin{pmatrix} \lambda_{11} & 1-\lambda_{11} \\ 1-\lambda_{11} & \lambda_{11} \end{pmatrix}$$

$$\lambda_{11} = \frac{1}{1-Y}; \quad Y(s) = \frac{g_{12}g_{21}}{g_{11}g_{22}}(s) \tag{1}$$

For $n \times n$ plants the RGA is defined by the ratio of the "open-loop" and "closed-loop" gains between input j and output i

$$\lambda_{ij} = \frac{(\partial y_i/\partial u_j)_{u_{l\neq j}}}{(\partial y_i/\partial u_j)_{y_{l\neq i}}} = g_{ij}(s)[G^{-1}(s)]_{ji} \tag{2}$$

Thus, the RGA matrix can be computed using the formula

$$\Lambda(s) = G(s) \times (G^{-1}(s))^T \tag{3}$$

where the $\times$ symbol denotes element by element multiplication (Hadamard or Schur product). The RGA matrix has some interesting algebraic properties (eg., Grosdidier et al., 1985):

a) It is scaling independent (eg., independent of units chosen for u and y). Mathematically, $\Lambda(D_1 G D_2) = \Lambda(G)$ where D_1 and D_2 are diagonal matrices.

b) All row and column sums equal one.

c) Any permutation of rows or columns in G results in the same pertubations in the RGA.

Another important usage of the RGA is that pairing on negative *steady-state* relative gains should be avoided. The reason is that with integral control this yields instability of either 1) the overall system, 2) the individual loop, or 3) the remaining system when the loop in question is removed. It is also established that plants with large RGA-values, in particular at high frequencies, are fundamentally difficult to control irrespective of the controller used (poor controllability).

A measure related to the RGA is the relative disturbance gain, RDG, introduced by Stanley et al. (1985). It was given a performance interpretation and extended to other

frequencies than zero by Skogestad and Morari (1987a). For loop i and a particular disturbance z_k, the RDG, β_{ik}, is defined as the ratio of the change in u_i needed for perfect disturbance rejection, to the change in u_i needed for disturbance rejection only in the corresponding output y_i (with all the other manipulated variables constant). We have

$$\beta_{ik} = \frac{(\partial u_i/\partial z_k)_{y_l}}{(\partial u_i/\partial z_k)_{y_i, u_{l\neq i}}} = \frac{[G^{-1}G_d]_{ik}}{g_{dik}/g_{ii}} \tag{4}$$

This formula also applies to non-zero frequencies. The RDG is also scaling independent and depends on the model of the plant and its disturbances. Note that the RDG has to be recomputed whenever another choice of pairings is selected, whereas the RGA need only be rearranged in accordance with the rearrangement of G.

A closely related disturbance measure, the closed loop disturbance gain (CLDG), was recently introduced by Skogestad and Hovd (1990). For a disturbance k and an output i, the CLDG is defined by

$$\delta_{ik}(s) = \beta_{ik}(s)g_{dik}(s) = g_{ii}(s)[G(s)^{-1}G_d(s)]_{ik} \tag{5}$$

The reason for the name CLDG will become clear later. A matrix of CLDG's may be computed from

$$\Delta = \{\delta_{ik}\} = \bar{G}G^{-1}G_d \tag{6}$$

The CLDG is scaling dependent, as it depends on the expected magnitude of disturbances and outputs. Actually, this is reasonable since CLDG is a performance measure, which generally are scaling dependent.

Notation

The controller $C(s)$ is diagonal with entries $c_i(s)$ (see Fig. 1). This implies that after the variable pairing has been determined, the order of the elements in y and u has been arranged so that the plant transfer matrix $G(s)$ has the elements corresponding to the paired variables on the main diagonal. Let $y(s)$ denote the output response for the overall system when all loops are closed and let $e(s) = y(s) - r(s)$ denote the output error. The closed loop response becomes

$$e(s) = -S(s)r(s) + S(s)G_d(s)z(s); \quad S = (I + GC)^{-1} \tag{7}$$

where $S(s)$ is the sensitivity function for the overall system , and z(s) denotes the disturbances. G is assumed to be a $n \times n$ square matrix, but G_d may be nonsquare. The matrix consisting of only the diagonal elements of $G(s)$ is denoted $\bar{G}(s)$, i.e., $\bar{G} = diag\{g_{ii}\}$. The Laplace variable s is often omitted to simplify notation.

2 Performance relationships

Assume that G and G_d have been scaled such that 1) the expected disturbances, $|z_k(j\omega)|$, are less or equal to one at all frequencies, and 2) the outputs, y_i are such that the expected setpoint changes, $|r_j(j\omega)|$, are less or equal to one.

Consider the effect of a setpoint change r_j and a disturbance z_k on the offset e_i. With all loops closed the closed-loop response becomes (Fig. 1)

$$e_i = -[S]_{ij}r_j + [SG_d]_{ik}z_k \tag{8}$$

For $\omega < \omega_B$ we may usually assume $S = (I + GC)^{-1} \approx (GC)^{-1}$. Provided the corresponding cofactor of G is nonzero,[1], and c_i is sufficiently large, this approximation will also hold for individual elements

$$[S]_{ij} \approx \frac{[G^{-1}]_{ij}}{c_i}; \quad [SG_d]_{ik} \approx \frac{[G^{-1}G_d]_{ik}}{c_i}; \quad \omega < \omega_B \tag{9}$$

With this approximation (8) becomes

$$e_i \approx -[G^{-1}]_{ij}\frac{1}{c_i}r_j + [G^{-1}G_d]_{ik}\frac{1}{c_i}z_k; \qquad \omega < \omega_B \tag{10}$$

If $g_{ji}(s) \neq 0$ and $g_{ii}(s) \neq 0$ the definitions of the RGA and CLDG yield $[G^{-1}]_{ij} = \lambda_{ji}/g_{ji}$ and $[G^{-1}G_d]_{ik} = \delta_{ik}/g_{ii}$ and we have

$$e_i \approx -\frac{g_{ii}}{g_{ji}}\frac{\lambda_{ji}}{g_{ii}c_i}r_j + \frac{\delta_{dik}}{g_{ii}c_i}z_k; \quad \omega < \omega_B \tag{11}$$

Using $\bar{S} = (I + \bar{G}C)^{-1}) \approx diag\{1/(g_{ii}c_i)\}$ this may be written on matrix form

$$e \approx -\bar{S}\bar{G}G^{-1}r + \bar{S}\bar{G}G^{-1}G_d z; \quad \omega < \omega_B \tag{12}$$

where $\bar{G}G^{-1}G_d = \Delta$ is the CLDG matrix. From (11) we see that the ratio $\lambda_{ii}/(g_{ii}c_i)$ gives the magnitude of the offset in output i to a setpoint change in this output. This ratio should preferably be small. That is, on a conventional magnitude Bode plot (log-log), the curve for $|\lambda_{ii}|$ should lie below $|g_{ii}c_i|$ at frequencies where we want small offsets. If we want e_j to be small when considering a change in setpoint i (small cross-interactions), we must also consider the offdiagonal elements in $\bar{G}G^{-1}$.

For process control disturbance rejection is usually more important than setpoint tracking. From (11) we see that the ratio $\delta_{ik}/(g_{ii}c_i)$ gives the magnitude of the offset in output i to a disturbance z_k. That is, the curve for $|\delta_{ik}|$ should lie below $|g_{ii}c_i|$ at frequencies where we want small offsets. A plot of $|\delta_{ik}(j\omega)|$ will give useful information about which disturbances k are difficult to reject.

Note that for input disturbances, i.e. $G_d = G$, we get $\delta_{ik} = g_{ii}$. Thus, large diagonal elements in G (when appropriately scaled) may imply difficulties rejecting input disturbances.

Comparison with all loops open. To get a better physical interpretation of the RGA and RDG consider the response $\bar{e}_i$ to a setpoint change r_i and a disturbance z_k when all the other loops are open. We get

$$\bar{e}_i = -(1 + g_{ii}c_i)^{-1}r_i + (1 + g_{ii}c_i)^{-1}g_{dik}z_k \tag{13}$$

At low frequencies we have $|g_{ii}c_i| \gg 1$ and derive

$$\bar{e}_i \approx -\frac{1}{g_{ii}c_i}r_i + \frac{g_{dik}}{g_{ii}c_i}z_k; \qquad \omega < \omega_B \tag{14}$$

Comparing (14) and (11) we see for a setpoint change r_i in loop i that λ_{ii} gives the approximate change in offset caused by closing the other loops. Similarly, for loop i and disturbance z_k we see that the the open-loop disturbance gain, g_{dik}, is replaced by the closed- loop disturbance gain, δ_{ik}. Also note that for disturbances $\beta_{ik} = \delta_{ik}/g_{dik}$ gives the approximate change in offset caused by closing the other loops.

[1] Cofactors of G identically equal to zero are relatively rare for transfer function matrices with dimension higher than 2×2, except for triangular transfer matrices.

2.1 Limitations of (11)

The main limitation with (11) is that it applies only to lower and intermediate frequencies. Furthermore, the issue of stability is not adressed.

Another limitation which we shall discuss in more detail here, is the assumption that all elements in $G(s)$ are nonzero. In particular, it is clear that relations involving $|g_{ii}c_i|$ in the denominator are not meaningful when $g_{ii} = 0$. Furthermore, it is well known that the RGA may be misleading for triangular $G(s)$, which have $\Lambda = I$. To better understand these limitations we shall consider the 2×2 case in detail. We have

$$(GC)^{-1} = \frac{1}{c_1c_2(g_{11}g_{22} - g_{12}g_{21})} \begin{pmatrix} g_{22}c_2 & -g_{12}c_2 \\ -g_{21}c_1 & g_{11}c_1 \end{pmatrix} \tag{15}$$

$$S = \frac{1}{c_1c_2(g_{11}g_{22} - g_{12}g_{21}) + 1 + g_{11}c_1 + g_{22}c_2} \begin{pmatrix} 1 + g_{22}c_2 & -g_{12}c_2 \\ -g_{21}c_1 & 1 + g_{11}c_1 \end{pmatrix} \tag{16}$$

All elements nonzero. In this case the approximation $S \approx (GC)^{-1}$ holds for all elements of S at frequencies where $|g_{11}c_1| \gg 1$ and $|g_{22}c_2| \gg 1$, which are then prerequisites (necessary conditions) for (11) to hold. The setpoint relationships in (11) become

$$\begin{aligned} e_1 &\approx -\frac{\lambda_{11}}{g_{11}c_1}r_1 - \frac{g_{11}}{g_{21}}\frac{\lambda_{21}}{g_{11}c_1}r_2 = -\frac{\lambda_{11}}{g_{11}c_1}(r_1 + \frac{g_{12}}{g_{22}}r_2) \\ e_2 &\approx -\frac{g_{22}}{g_{12}}\frac{\lambda_{12}}{g_{22}c_2}r_1 - \frac{\lambda_{22}}{g_{22}c_2}r_2 = -\frac{\lambda_{11}}{g_{22}c_2}(\frac{g_{21}}{g_{11}}r_1 + r_2) \end{aligned} \tag{17}$$

Zero diagonal elements in G. Without loss of generality consider the case $g_{11} = 0$ (and $\lambda_{11} = \lambda_{22} = 0, \lambda_{12} = \lambda_{21} = 1$. Then (11) for loop 1 in terms of $g_{11}c_1$ is meaningless. Furthermore, to derive (11) for loop 2 we assumed $|g_{11}c_1| \gg 1$ in (9), but this of course not possible for $g_{11} = 0$. We therefore conclude that if $g_{11} = 0$ then (11) does not apply neither to loop 1 or 2. For (9) to hold in this case we must require

$$|g_{22}c_2| \gg 1; \quad |c_1| \gg |\frac{g_{22}}{g_{12}g_{21}}| \tag{18}$$

The performance relationships for setpoint tracking to replace (17) become

$$\begin{aligned} e_1 &\approx -\frac{g_{22}}{g_{12}g_{21}}\frac{1}{c_1}r_1 - \frac{1}{g_{21}}\frac{1}{c_1}r_2 \\ e_2 &\approx -\frac{g_{22}}{g_{12}}\frac{1}{g_{22}c_2}r_1 - \frac{1}{g_{12}g_{21}}\frac{1}{c_1c_2}r_2 \end{aligned} \tag{19}$$

The last term puts a requirement on the product of the controller gains. This is reasonable since with $g_{11} = 0$ input u_1 can only affect output y_1 by the indirect action of control loop 2. For disturbance rejection, (11) holds provided (18) holds.

Zero offdiagonal elements in $G(s)$ ($G(s)$ triangular). (17) (with $\lambda_{11} = 1$) holds also in this case. The important point to note is that interactions may cause poor performance in spite of the fact that $\Lambda = I$. For example, when $g_{12} = 0$ interactions from r_1 to e_2 may be severe if $|g_{21}/g_{11}|$ is large.

2.2 Summary

Let us at this point summarize some results we shall use in the examples:

Pairing Rule 1. Avoid pairings ij with negative values of the steady-state RGA, $\lambda_{ij}(0)$ (Grosdidier et al., 1985).

Pairing Rule 2. Prefer pairings which yield the RGA-matrix close to identity (the rule follows from considering overall stability, note that it is not sufficient to check only if the diagonal elements are close to 1, see Hovd and Skogestad (1990).

Pairing Rule 3. Prefer pairings ij where $g_{ij}(s)$ puts minimal restrictions on the achievable bandwidth for this loop (the rule follows from (11) above).

Rule 3 is the conventional rule of pairing on variables "close to each other". Rules 1-3 will in many cases determine the best choice of pairings for decentralized control. To evaluate controllability we shall use:

Controllability Rule 1. Avoid plants (designs) with large RGA-values (in particular at frequencies near cross-over). This rule applies for any controller, not only to decentralized control (Skogestad and Morari, 1987b).

Controllability Rule 2. For decentralized control avoid control structures (an entire *set* of pairings) with large values of $|\delta_{ik}|$ in the crossover region, and in particular if the achievable bandwidth for the corresponding loop i is restricted (because of $g_{ii}(s)$, see pairing rule 2) (the rule follows from (11) above).

3 Distillation Control

From a control point of view distillation columns may be considered as a 5×5 system with inputs u and outputs y.

$$u = (L, V, D, B, V_T)^T \tag{20}$$

$$y = (y_D, x_B, M_D, M_B, p)^T \tag{21}$$

The model in terms of deviation variables is

$$y(s) = G(s)u(s) \tag{22}$$

The number of possible pairings for single-loop control is very large. However, in most cases condenser duty, V_T, is used to control pressure, p, and we have a 4×4 control problem. The 4×4 RGA-matrix for this case has a 2×2 identity matrix in the lower right corner, and a 2×2 full matrix in the upper left corner. Intuitively, one would then expect the pairings suggested by the order of (20) and (21) to be preferred. This would yield the LV-configuration where L and V are used for composition control. However, industrial experience have suggested that other options may be preferable, and this is studied below.

The term configuration used below refers to the two independent variables used for composition control. The two level loops are assumed to be closed, and with perfect control. Note that the RGA of the remaining 2×2 problem for composition control (with

level loops closed) in general is quite different from the RGA-matrix of the original open-loop system in (22).

We shall next study the following: 1) Compostion control with LV configuration, 2) Top part of column for DV-configuration, 3) Composition control with other configurations.

3.1 Example 1: Composition control with LV configuration

In order to demonstrate the use of the frequency dependent RGA and CLDG for control structure selection and evaluation of expected control performance, a binary distillation column with 40 theoretical trays plus a total condenser is considered. This is the same column as studied by Skogestad et al. (1988), but we use a more rigorous model which includes liquid dynamics in addition to the composition dynamics. The model has a total of 82 states. Disturbances in feed flowrate F (z_1) and feed composition z_F (z_2), are included in the model. The LV configuration is used, that is, the manipulated inputs are reflux L ($u_1 = L$) and boilup V ($u_2 = V$). Outputs are the product compositions y_D (y_1) and x_B (y_2). The model then becomes

$$\begin{pmatrix} dy_1 \\ dy_2 \end{pmatrix} = G(s) \begin{pmatrix} du_1 \\ du_2 \end{pmatrix} + G_d(s) \begin{pmatrix} dz_1 \\ dz_2 \end{pmatrix} \tag{23}$$

The steady state gain matrices are

$$G(0) = \begin{pmatrix} 87.8 & -86.4 \\ 108.2 & -109.6 \end{pmatrix}; \quad G_d(0) = \begin{pmatrix} 11.8 & 17.6 \\ 17.6 & 22.4 \end{pmatrix} \tag{24}$$

The disturbances and outputs have been scaled such that a magnitude of 1 corresponds to a change in F of 30%, a change in z_F of 20%, and a change in x_B and y_D of 0.01 molefraction units.

Pairings. Rule 1 dictates that one should use u_1 to control y_1 and u_2 to control y_2, as indicated by (23). This is in agreement with industrial practice.

Analysis of the model. Fig. 2 shows the open-loop disturbance gains, g_{dik}, as a function of frequency. These gains are quite similar in magnitude and rejecting disturbances z_1 and z_2 seems to be equally difficult. However, this conclusion is incorrect. The reason is that the *direction* of these two disturbances is quite different, that is, disturbance 2 (z_F) is well aligned with G and is easy to reject, while disturbance 1 (F) is not (Skogestad and Morari, 1987a). This is seen from Fig. 3 where the closed-loop disturbance gains, δ_{i2}, for z_2 are seen to be much smaller than δ_{i1} for z_1.

Observed control performance. To check the validity of the above results we used the single-loop PI controllers by Skogestad et al. (1990).

The loop gains, $|g_{ii}c_i|$, with these controllers are also shown in Fig. 3. The loop gain for the top composition is smaller than the closed-loop disturbance gain, $|\delta_{11}|$, at frequencies close to crossover, while the bottom composition loop gain is larger than $|\delta_{2k}|$ at all frequencies. Closed-loop simulations with these controllers are shown in Fig. 4. The simulations confirm that disturbance 2 is much easier rejected than disturbance 1. They also confirm that with these controller settings, a disturbance in F has a larger effect on y_D than on x_B. In summary, there is an excellent correlation between the analysis based on $|\delta_{ik}|$ in Fig. 3 and the simulations. This is not surprising when one considers Fig. 5 which shows the accuracy of the approximation $[S(s)G_d(s)]_{ik} \approx \frac{\delta_{ik}(s)}{g_{ii}(s)c_i(s)}$ which was used to derive Eq.(11) and which formed the basis for the analysis in Fig. 3. The approximation

is very good at low frequencies, but as expected poorer at frequencies around the closed loop bandwidth.

3.2 Example 2: Top part of column with DV-configuration

In order to demonstrate that acceptable control may be achieved even with pairings corresponding to $\lambda_{ii} = 0$, consider control of the top part of a distillation column. It is desired to control the top product composition (y_D) and the level in the condenser (M_D). The manipulated inputs are the distillate flowrate (D) and the reflux flowrate (L). The vapor flowrate entering the top of the column is considered to be the only disturbance (V_T). After scaling, the resulting transfer functions are

$$\begin{pmatrix} dy_D \\ dM_D \end{pmatrix} = \begin{pmatrix} 0 & \frac{100}{1+100s} \\ \frac{-1}{s} & \frac{-1}{s} \end{pmatrix} \begin{pmatrix} dD \\ dL \end{pmatrix} + \begin{pmatrix} \frac{-100}{1+100s} \\ \frac{1}{s} \end{pmatrix} dV_T \tag{25}$$

This pairing corresponds to $\lambda_{11} = \lambda_{22} = 0$ at all frequencies. This pairing may be preferred in some cases, for example, if the reflux is large such that constraints on the distillate flowrate make level control with this input difficult. We shall show that stability and performance may be achieved even with this pairing. The achieveabe bandwidth is limited by unmodeled measurement delay in y_D of one minute and and valve dynamics in L equivalent to a time delay of 0.1 minute. The chosen controllers are

$$c_1(s) = -0.5\frac{1+10s}{10s}; \quad c_2(s) = -5 \tag{26}$$

Stability of the individual loops and overall stability is achieved. To check performance, the controllers and the bounds (17) for the case with zero diagonal elements are shown in Fig. 6. As the ratio of $|g_{22}c_2|$ to $|\delta_{21}|$ is constant (= 5) and does not approach infinity at steady state, a step in the disturbance will not be perfectly rejected in loop 2. The bounds in Fig. 6 indicate that interactions put no serious limitations on achievable performance. In Fig. 7 we show responses to changes in setpoints r_1 and r_2 and in disturbance z_1. In the simulations a first order filter with a time constant of one minute is used for both setpoints, and a one minute time delay in the measurement of y_1 and a 0.1 minute time delay in manipulated variable u_2 are approximated with first order Padé approximations. The observed control performance is satisfactory, although there is an undesirable interaction from setpoint r_2 to output y_1. This interaction cannot be predicted from Fig. 6, as Eq. (9) does not hold in the crossover region where the interactions occur.

3.3 Example 3: Composition control with other configurations

The model for various configurations

$$LV, DV, (L/D)(V/B), DB, LB$$

was obtained from (22) by closing the level loops assuming perfect control. For example, for the DV-configuration we need D instead of L as an independent variable. Perfect

control of condenser level gives:

$$L(s) = V(s) - D(s) \tag{27}$$

The different configurations are described in more detail in Skogestad et al. (1990) where controller tunings also are given. The RGA-values for the five configurations are shown in Fig. 8. In Fig. 9 we show the CLDG's together with the loop gains obtained by Skogestad et al. (1990). Overall, the CLDG's are not very different for the various configurations, but the loop gains are different because of the effect of interactions (e.g. λ_{11}) on stability. Comparing Fig. 9 with the closed-loop simulations in Fig. 10 we note an excellent agreement. From the CLDG's we can easily identify the worst disturbance for each configuration: Feed rate for LV, feed composition for (L/D)(V/B) and similar sensitivity to feed rate and feed composition disturbances for DB. The LB and DV configurations combine the closed loop disturbance gains of the LV and DB configurations in two different ways. The top composition in LB is sensitive to disturbances in F (similar to LV), the bottom composition is equally sensitive to disturbances in F and z_F (similar to DB). For DV the CLDG's for the top composition are similar to those for DB, and the CLDG's for the bottom composition are similar to those for LV.

4 Example 4: Control of a Fluid Catalytic Cracker

The Fluid Catalytic Cracking (FCC) process is an important process for upgrading the heavy components of crude oil in refineries. A overview of a typical FCC is shown in Fig. 11. Typically, the control problem is to use as manipulated inputs

F_a - flow rate of air to the regenerator

F_s - flow rate of regenerated catalyst to the riser reactor

to control the outputs

O_f - the amount of oxygen in the flue gas

T - some temperature

The amount of oxygen in the flue gas needs to be controlled to avoid combustion of carbon monoxide to carbon dioxide in the piping and equipment downstream the regenerator, which can result in a large temperature rise and cause structural damage. In addition either the riser exit temperature T_{ri} or the regenerator temperature T_{rg} is used to control the cracking reaction in the riser in order to get the desired product split. Advanced Model Predictive Control (MPC) type of control is known to be installed on some FCC units, but many units still use traditional decentralized control. Where decentralized control is used, the pairings indicated above are most often used.

4.1 Modeling of the FCC process

Unlike what is the case for distillation columns, relatively little has been published on the modeling and control of FCC's. The main reason for this is that licensing companies and operating companies have been reluctant to give out much information about the process. It is therefore difficult to assess how well the limited number of published simulation models describe the behaviour of actual FCC processes. We shall use the model of Lee and Groves (1985), as we believe this is the model which best describes modern FCC's. Readers are referred to this paper or to Ljungquist (1990) for a complete description of the model, as

the objective of this example is to demonstrate the use of the RGA and CLDG, and not to describe models for simulation of the FCC process.

The model of Lee and Groves has been implemented in a simulation program and numerical differentiation is used to obtain a linear model.

4.2 Choice of control structure

Two different control structures for control of FCC's have been proposed. They are:

1. Conventional control structure: F_s (flowrate of regenerated catalyst) is used to control T_{ri} (the riser exit temperature).
2. Kurihara control structure: F_s is used to control T_{rg} (the regenerator temperature) (Kurihara, 1967).

Both structures use F_a to control O_f (the concentration of oxygen in the flue gas). In the model used in this work, only the oxygen concentration in the regenerator O_d is available, and it is therefore used instead of the concentration in the flue gas. The same simplification is implicit in much of what has been published previously on the control of FCC's.

For the model used in this work, the transfer function matrix from manipulated variables to outputs for the conventional control structure has transmission zeros at $0.02min^{-1}$ and $0.2min^{-1}$, whereas the transfer function matrix for the Kurihara control structure has a transmission zero at $0.3min^{-1}$. Since the smallest (in magnitude) RHP-zero limits the achievable closed-loop bandwidth, the Kurihare structure is perferable from this point of view and we decided to use the Kurihara structure in the following.

4.3 Choice of pairings

Note that the term "control structure" as used above includes both the choice of controlled ouputs ($T = T_{ri}$ for conventional structure and $T = T_{rg}$ for Kurihara) *and* the choice of pairings (both structures above use F_a to control O_d and F_s to control T).

Interestingly, we found that both proposed control structures correspond to pairing on negative relative gains, that is, do not satisfy *pairing rule 1.* [2] This means that for the Kurihara control structure, one of the control loops must be unstable by itself for the whole control structure to be stable. Since stability of the individual loops is highly desireable, we decided to also study the Kurihara structure with reverse pairings.

Furthermore, the Kurihara structure also violates *pairing rule 3*, as the transfer function from F_s to T_{rg} has a rhp zero at $0.0011min^{-1}$ and the transfer function from F_a to O_d has a rhp zero at $0.2min^{-1}$. With the reversed pairing there are no rhp zeros in either of the transfer function pairings within a realistically achieveable bandwidth.

4.4 Analysis using frequency dependent RGA and CLDG

In the following consider the Kurihara case and let $y_1 = O_d$ and $y_2 = T_{rg}$. The transfer functions for the process and disturbances were scaled to make the maximum expected setpoint changes and the maximum magnitude of disturbances all equal one. The maximum changes in the setpoints (i) assumed in this example is

[2] We are somewhat surprised to find that both these industrially used control structures correspond to pairing on negative $\lambda_{ij}(0)$. It is not clear whether this is really the case or the result of errors in the model used in this work.

1. y_{1s} - oxygen concentration in regenerator: 0.001 molefraction.
2. y_{2s} - regenerator temperature: 5 K.

The maximum magnitudes of the disturbances (k) are assumed to be

1. Temperature of air to regenerator: 5 K.
2. Flowrate of gas oil to riser: 2 kg/s.
3. Rate of formation of coke: 2.5% relative to original value.
4. Temperature of gas oil to riser: 5 K.

For λ_{ij} and δ_{ik} the subscript i refers to the number of the setpoint or measurement and the subscript k refers to the number of the disturbance as listed above.

Kurihara structure with reverse pairings.

In this case $u_1 = F_s$ and $u_2 = F_a$. Figures 12a and 12b show $\lambda_{ii}(j\omega)$, $\delta_{ik}(j\omega)$ and the loop gains for loop 1 ($i = 1$) and loop 2 ($i = 2$), respectively. It is clear that with the chosen scalings, disturbance 2 (the oil flowrate) is the most difficult to reject, and disturbance 1 (the air temperature) is the easiest to reject in both outputs. Also shown in figures 12a and 12b are the loop gains for loop 1 and 2 respectively, and $\lambda_{ii}(j\omega)$ which is equal for both loops. The (scaled) controllers used in this work are:

$$c_1(s) = -50\frac{(166.7s+1)}{166.7s} \tag{28}$$

$$c_2(s) = 10\frac{(166.7s+1)}{166.7s} \tag{29}$$

where the integral time is given in minutes. Comparing the loop gains to the $\delta_{ik}(j\omega)$'s indicates that disturbance 2 could have some effect on y_1 (the oxygen concentration), whereas the other disturbances appear easy to reject.

Kurihara structure.

In this case $u_1 = F_a$ and $u_2 = F_s$. The CLDG's of the Kurihara control structure are not shown here, but such a plot would again show that disturbance 2 is most difficult to reject and a disturbance 1 is easiest to reject. Also, for the controller parameters used by Lee and Groves (1985), disturbance 2 would affect y_2 more than y_1.

4.5 Comparison with simulation results

Figures 13 and 14 show simulations for disturbance 1 (an increase in the air temperature of 5 K) and disturbance 2 (an increase in the oil flowrate of 2 kg/s), respectively. The solid lines are for the reverse Kurihara structure with controller tunings given above, whereas the dotted line are obtained using the Kurihara control structure with the controller parameters of Lee and Groves (1985).

The predictions based on the CLDG are in excellent agreement with the results from the simulations. For both control structures disturbance 2 is much worse than disturbance 1. As predicted by the CLDG's, disturbance 2 mostly affects y_1 for our controller and y_2 for Lee and Groves' controller.

The performance of both controllers are comparable; Lee and Groves' controller achieves better control of y_1 (the oxygen concentration) whereas our controller controls y_2 (the regenerator temperature) better. The reason is that the transmission zero at $0.3min^{-1}$ is

mainly in the direction of the second input, F_s. Thus it mainly limits the achievable bandwidth for y_2 with the Kurihara control structure, whereas it mainly limits the achievable bandwidth for y_1 with our reverse Kurihara structure. One important additional advantage with our controller is that it remains stable if one of the control loops is taken out of service, whereas for the Kurihara control structure with the controller parameters used by Lee and Groves the regenerator temperature control loop is unstable by itself.

5 Example 5: Limitations with performance relationships

This example is intended to illustrate that the performance relationships derived above may be misleading as constraints and stability considerations are not included. Consider the the following process

$$G(s) = \frac{1}{10s+1}\begin{pmatrix} 1 & -0.1 \\ 0.1 & 1 \end{pmatrix} \tag{30}$$

with λ_{11} at all frequencies equal to 0.99. We shall consider using both this pairing (denoted pairing A) and the reverse pairing (denoted B). Assume that the control problem is to reject input disturbances. Then the CLDG-matrix is equal to $\bar{G}$, and one might conclude that it is best to pair on small elements in G and that pairing B is preferred. This conclusion follows if one designs controllers for the two cases with the same bandwidth in the individual loops. For case A

$$c_1(s) = 1\frac{10s+1}{10s} \tag{31}$$

For the reverse pairing, B, we get 10 times higher gains in the controller. The responses are simulated in Fig. 15, and we see that the response in terms of offset (y) is indeed best for the reverse pairing, B. However, the response is strongly oscillatory, and would probably be unstable in practice because of time delays etc. We also note that the inputs are much larger and one might hit input constraints in case B. There is also a large peak in the sensitivity function as seen in Fig. 16.

The reason why the response with the reverse pairing, B, is better (at least in terms of offset) is as follows: The individual loops are tuned to be equally fast. For the original pairing the loop gain is essentially unaltered as the two loops are closed simultaneously. However, the reverse pairing corresponds to $\lambda_{11} = 0.01$, that is, interactions between the loops cause the effective loop gains to be about 100 times larger when both loops are closed. This increased loop gain gives better disturbance rejection.

However, in practice the reverse pairing will probably not be used. First, it goes against pairing rule 2 and will most probably yield instabilty (unless the tunings are changed, for example, by making one loop fast and one slow). Second, it may not perform as well in practice because of input constraints.

6 Conclusions

In the paper we have derived performance relationships for the overall system in terms of the individual loops. Importantly, the relationships depend on the model of the process only, that is, are independent of the controller. This means that frequency-dependent

plots of λ_{ii} and δ_{ik} may be used to evaluate the achievable closed-loop performance (controllability) under decentralized control. Plants with small values of these measures are preferred. Furthermore, the values of δ_{ik} may tell the engineer which disturbance k will be most difficult to handle using feedback control. This may pinpoint the need for using feedforward control, or for modifying the process. For example, in process control adding a feed buffer tank will dampen the effect of disturbances in feed flowrate and composition. Plots of δ_{ik} may be used to tell if a tank is necessary and what holdup (residence time) would be needed.

The bounds may be used to obtain a first guess of the controller parameters. However, as the derivation of the bounds depends on approximations which are valid at low frequencies only, undesirable effects may occur at frequencies around the closed loop bandwidth. Thus the behavior of the closed-loop system must be checked using other methods, and the controllers possibly redesigned.

Acknowledgements. Support from NTNF is gratefully acknowledged.

Nomenclature (also see Section 1 and Fig. 1)

$e = y - r$ - vector of offsets
$g_{ij} = [G]_{ij}$ - ij'th element of G
$g_{dik} = [G_d]_{ik}$ - ik'th element of G_d
G^{ij} - G with row i and column j removed
r - vector of reference outputs (setpoints)
u - vector of manipulated inputs
y - vector of outputs
$Y = \frac{g_{12}g_{21}}{g_{11}g_{22}}$ - Rijnsdorp or Balchen interaction measure for 2×2 system
z - vector of disturbances
β_{ik} - ik'th element of RDG matrix
$\delta_{ik} = g_{ii}[G^{-1}G_d]_{ik} = [\bar{G}G^{-1}G_d]_{ik} = beta_{ik}g_{dik}$ - Closed Loop Disturbance Gain
$\lambda_{ij}(G) = g_{ij}[G^{-1}]_{ji}$ - ij'th element in RGA-matrix Λ
Λ - RGA matrix
ω - frequency
ω_B - closed loop bandwidth

Subscripts
i - index for outputs or loops
j - index for manipulated inputs or setpoints
k - index for disturbances

References

Balchen, J. G. and Mumme, K. , 1988 *Process Control. Structures and Applications*, Van Nostrand Reinhold, New York.

Bristol, E.H., 1966, "On a new measure of interactions for multivariable process control", *IEEE Trans. Automat. Control*, **AC-11**, 133-134.

Bristol, E.H., 1978, "Recent results on interactions in multivariable process control", Paper at AIChE Annual Meeting, Chicago, IL.

Grosdidier, P., Morari, M. and Holt, B.R., 1985, "Closed-Loop Properties from Steady-State Gain Information", *Ind. Eng. Chem. Fundam.*, **24**, 221-235.

Hovd, M. and Skogestad, S., 1990, "Use of Frequency-Dependent RGA for Control System Analysis, Structure Selection and Design", Accepted for publication in *Automatica*.

Kurihara, H., 1967, "Optimal Control of Fluid Catalytic Cracking Processes", *MIT Electr. Sys. Lab.*, report ESL-R-309.

Lee, E. and Groves, F. R., Jr., 1985, "Mathematical Model of the Fluidized Bed Catalytic Cracking Plant", *Trans. Soc. Comp. Sim.*, **2**, no. 3, pp. 219-236.

Ljungquist, D., 1990, Ph.D. Thesis, Norwegian Institute of Technology.

Shinskey, F.G., 1967, *Process Control Systems*, McGraw-Hill, New York.

Shinskey, F.G., 1984, *Distillation Control*, 2nd Edition, McGraw Hill, New York.

Skogestad, S. and Morari, M., 1987a, "Effect of Disturbance Directions on Closed Loop Perfomance", *Ind. Eng. Chem. Res.*, **26**, 2029-2035.

Skogestad, S. and Morari, M., 1987b, "Implications of Large RGA Elements on Control Performance", *Ind. Eng. Chem. Res.*, **26**, 11, 2323-2330.

Skogestad, S. and Morari, M., 1988, "Variable selection for decentralized control", Paper at *AIChE Annual Meeting*, Washington DC.

Skogestad, S., Morari, M. and Doyle, J.C, 1988, "Robust Control of Ill- Conditioned Plants: High Purity Distillation", *IEEE Trans. Autom. Control*, **33**, 12, 1092-1105.

Skogestad, S., Lundström, P. and Jacobsen, E.W., 1990, "Selecting the best distillation control configuration", *AIChE Journal*, **36**, 5, 753-764.

Skogestad, S. and Hovd, M., 1990, "Use of frequency-dependent RGA for control structure selection", Paper at *American Control Conference*, San Diego CA.

Stanley,G., Marino-Galarraga, M., McAvoy, T.J., 1985, "Shortcut operability analysis. 1. The relative disturbance gain. *Ind. Eng. Chem. Process Des. Dev.*, **24**, 4, 1181-1188.

FIGURES

1. **Figure 1**. Block diagram of decentralized control structure.
2. **Figure 2**. Open loop disturbance gains, g_{dik}, for LV configuration.
3. **Figure 3**. Closed loop disturbance gains, δ_{ik}, and loop gains, $g_{ii}c_i$, for LV configuration. Top: top composition. Bottom: bottom composition.
4. **Figure 4** Responses to a 30% increase in F at $t = 0$ and a 20% increase in z_F at $t = 50$min. Solid curve: top composition, y_D. Dashed curve: bottom composition, x_B.
5. **Figure 5** Check of approximation (9) for Example 1. The figure shows the magnitude of $[SG_d]_{ik}/(\frac{\delta_{ik}}{g_{ii}c_i})$
6. **Figure 6** Bounds on controller and loop gains for Example 2.
7. **Figure 7** Responses for Example 2 to unit step changes in r_1 at $t = 0$, in r_2 at $t = 40$, and in z_1 at $t = 80$. Solid line: y_1, dashed line: y_2.
8. **Figure 8** RGA-values, $|\lambda_{11}(j\omega)|$, for the five configurations.
9. **Figure 9** Closed loop disturbance gains, δ_{ik}, and loop gains, $g_{ii}c_i$, for various configurations. Top: top composition. Bottom: bottom composition.
10. **Figure 10** Responses to a 30% increase in F at $t = 0$ and a 20% increase in z_F at $t = 50$min. Solid curve: top composition, y_D. Dashed curve: bottom composition, x_B.
11. **Figure 11** Overview of typical FCC plant.
12. **Figure 12** Closed loop disturbance gains, δ_{ik}, relative gain λ_{ii} and loop gain $g_{ii}c_i$ for example 4. Figures 12a and 12b show the bounds for $i = 1$ and $i = 2$ respectively.
13. **Figure 13** Response to an increase in the air temperature of 5 K.
14. **Figure 14** Response to an increase in the feed oil flowrate of 2 kg/s.
15. **Figure 15** Responses to a unit step disturbance in input 1 for pairing A and input 2 for pairing B. Top: output responses. Bottom: input responses.
16. **Figure 16** Sensitivity functions for pairing A (top) and pairing B (bottom).

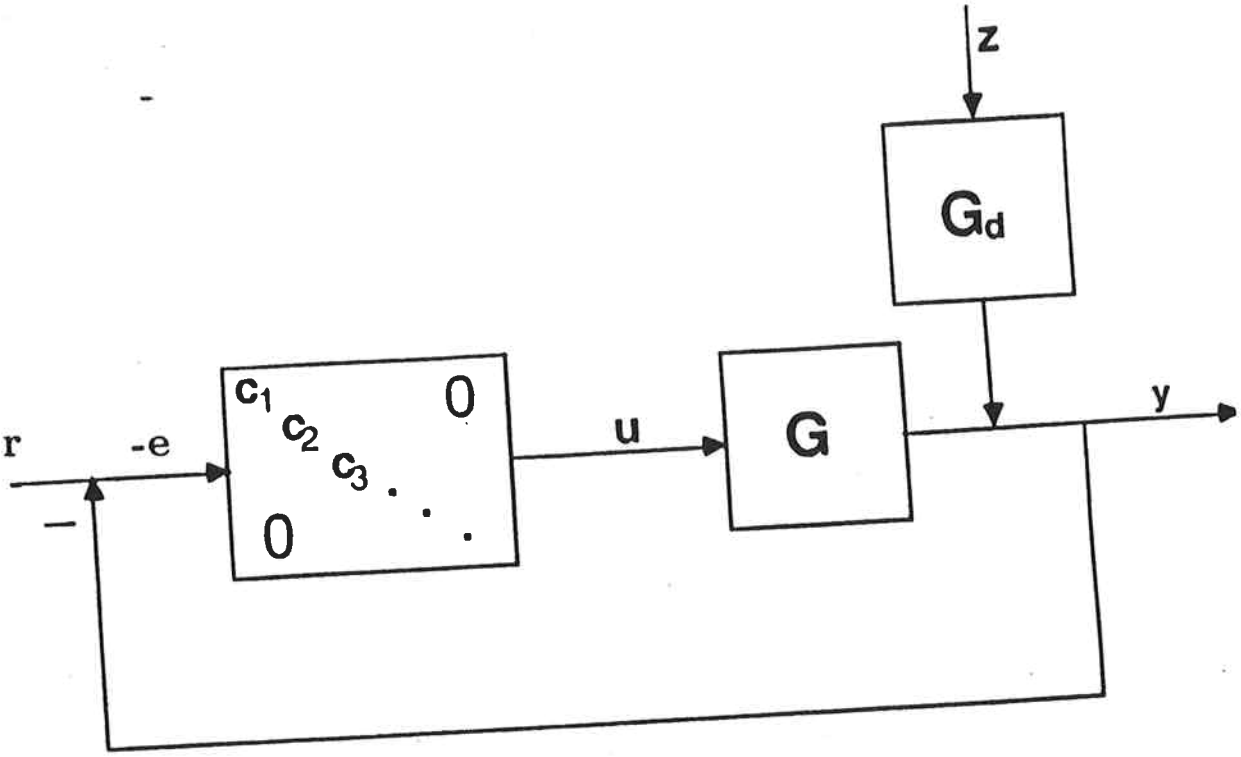

Figure 1. Block diagram of decentralized control structure.

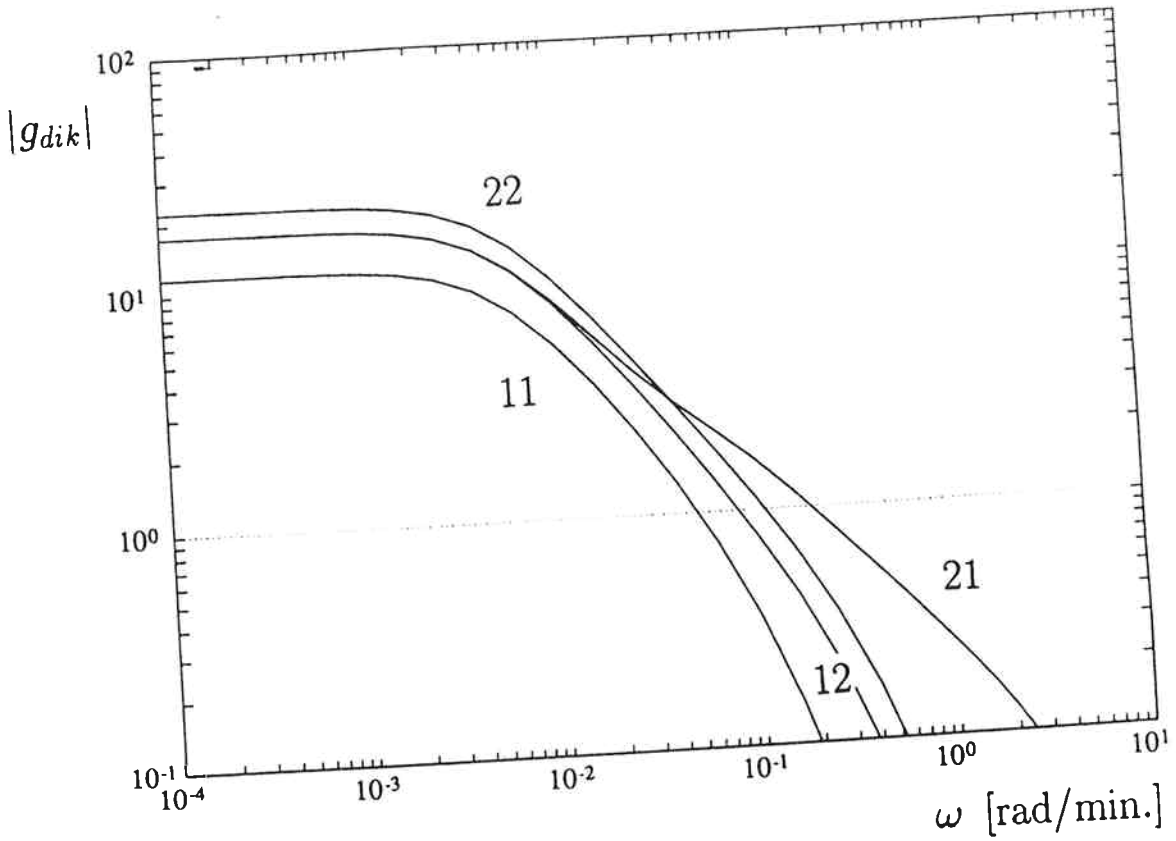

Figure 2. Open loop disturbance gains, g_{dik}, for LV configuration.

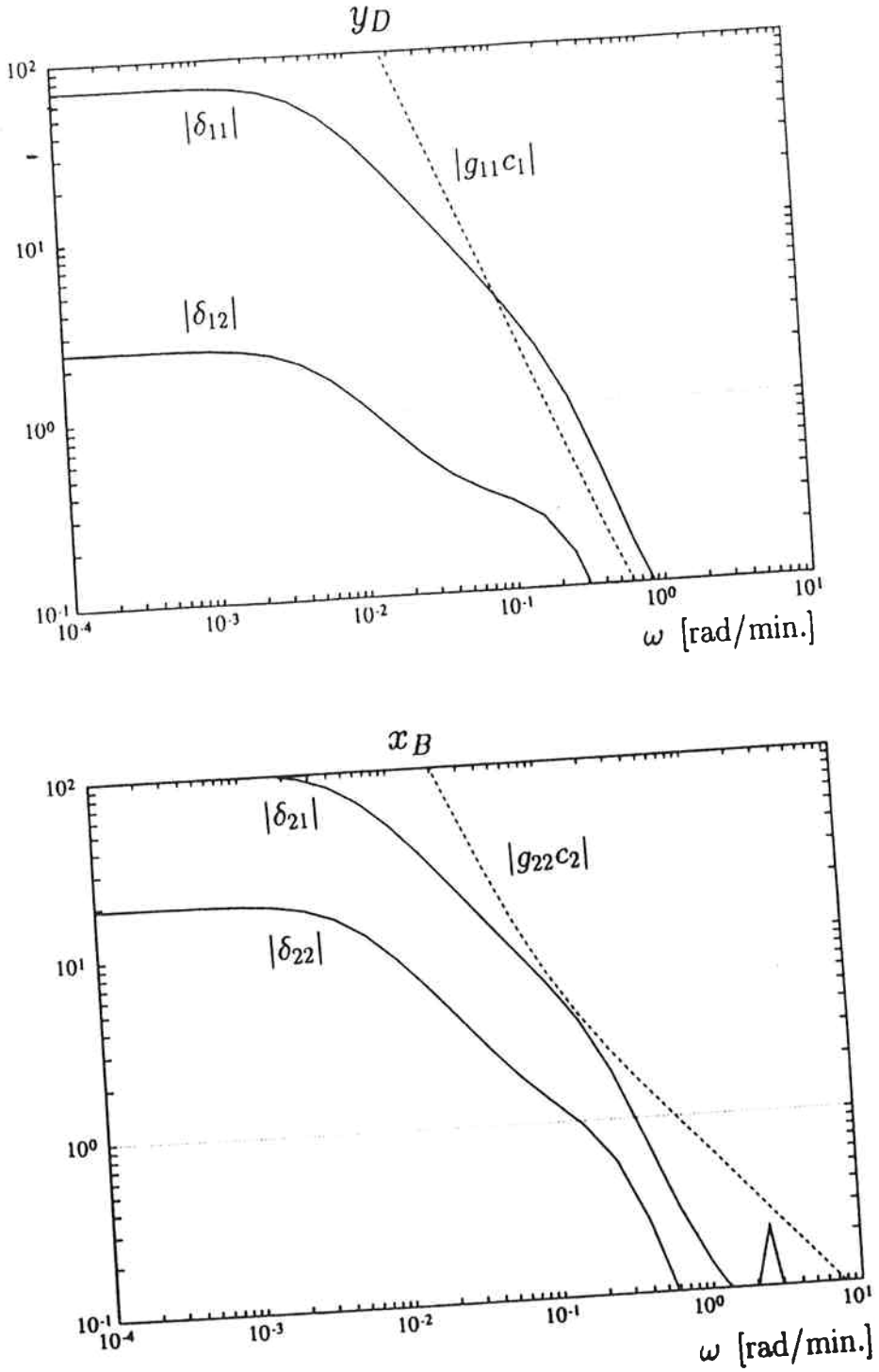

Figure 3. Closed loop disturbance gains, δ_{ik}, and loop gains $g_{ii}c_i$, for LV configuration.

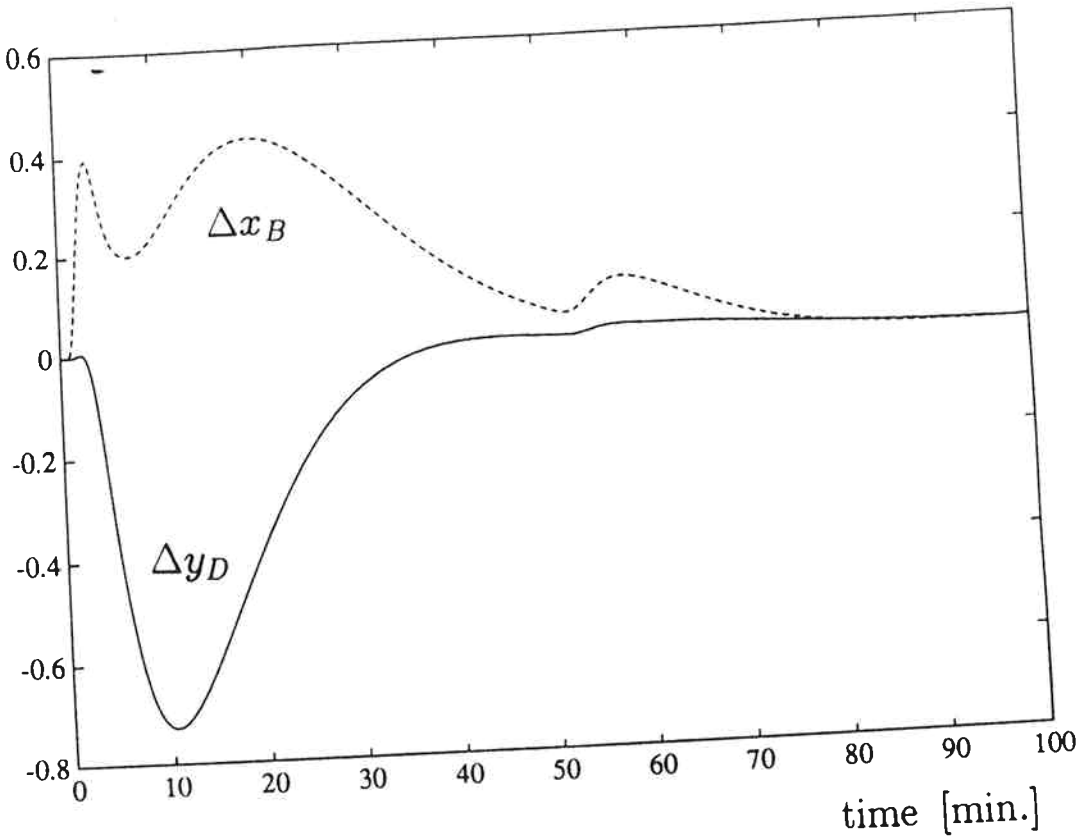

Figure 4 Responses to a 30% increase in F at $t = 0$ and a 20% increase in z_F at $t = 50$min.

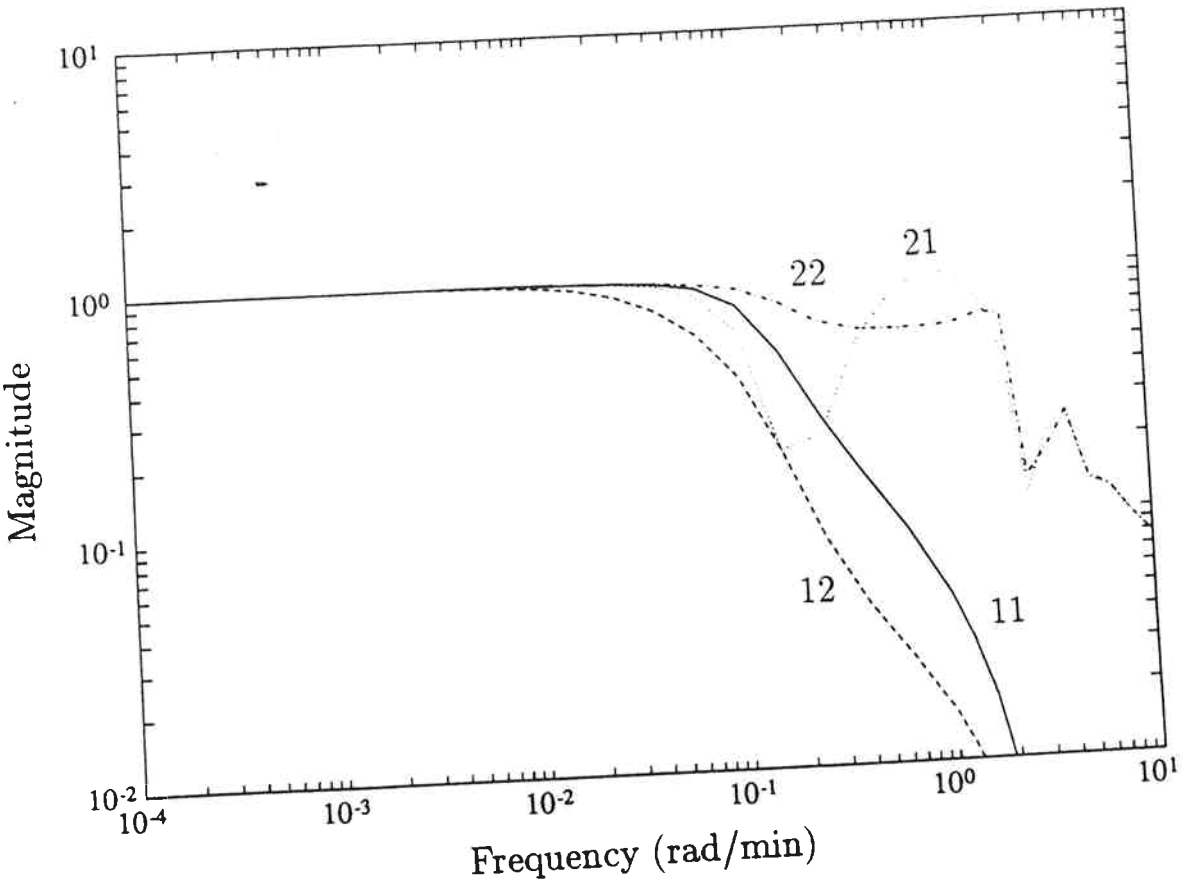

Figure 5 Check of approximation (9) for Example 1. The figure shows the magnitude of $[SG_d]_{ik}/(\frac{\delta_{ik}}{g_{ii}c_i})$.

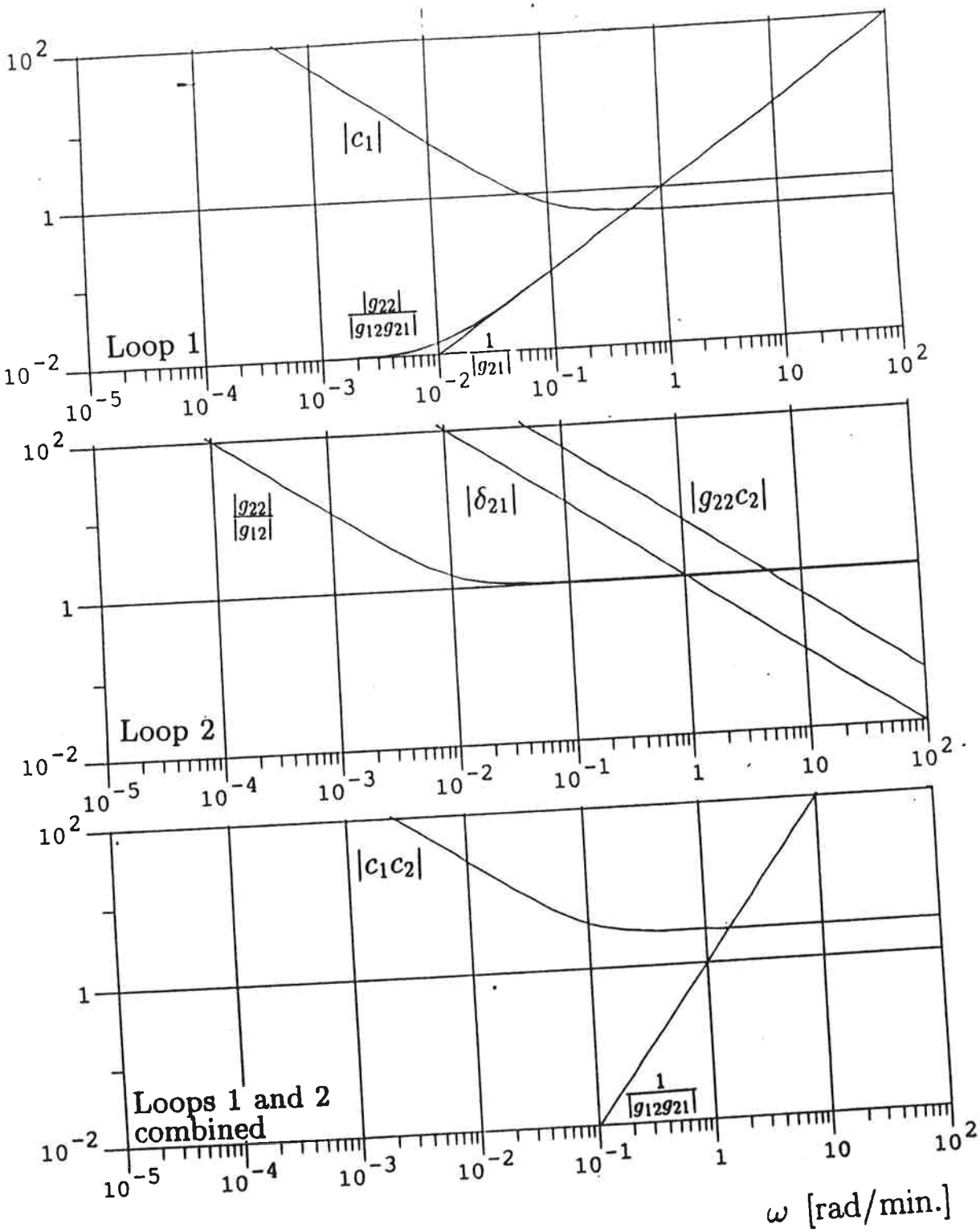

Figure 6. Bounds on controller and loop gains for Example 2.

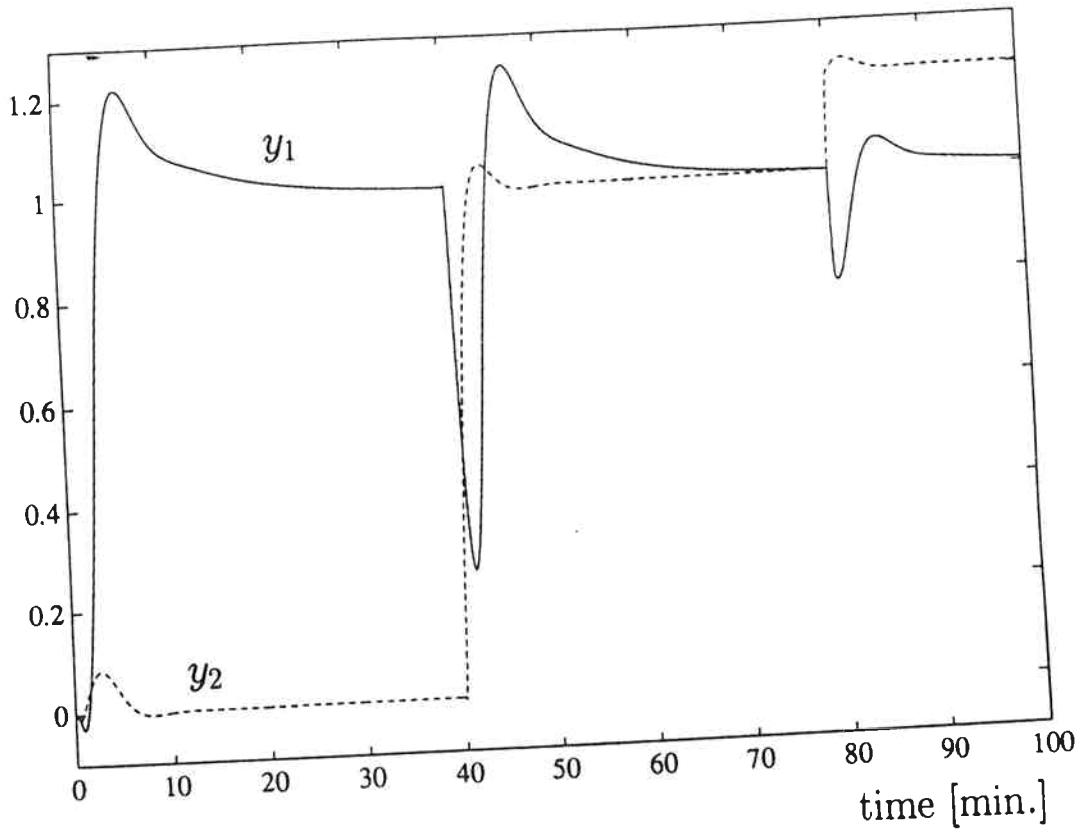

Figure 7. Responses for Example 2 to unit step changes in r_1 at $t = 0$, in r_2 at $t = 40$, and in z_1 at $t = 80$.

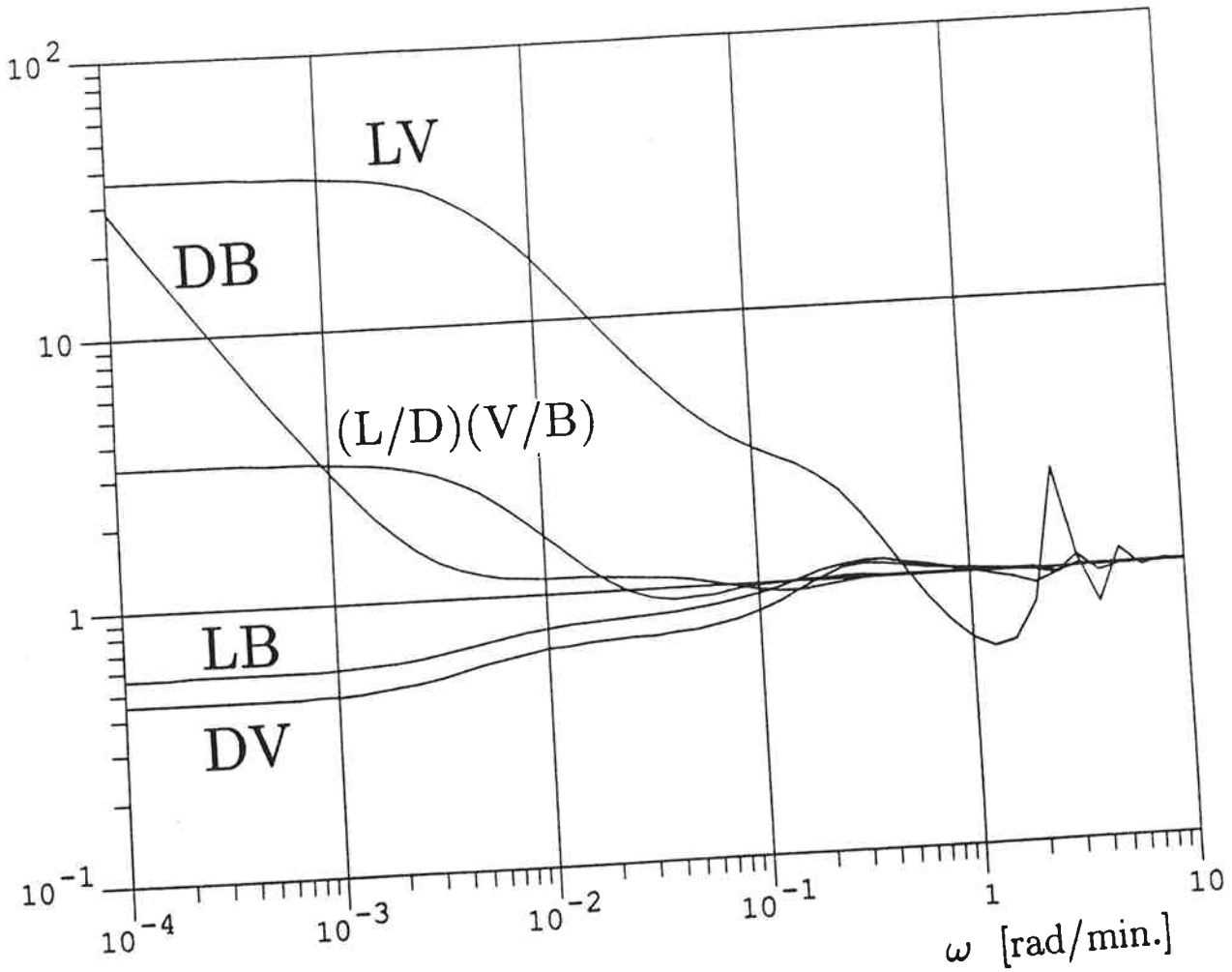

Figure 8. RGA-values, $|\lambda_{11}(j\omega)|$, for the five configurations.

DB

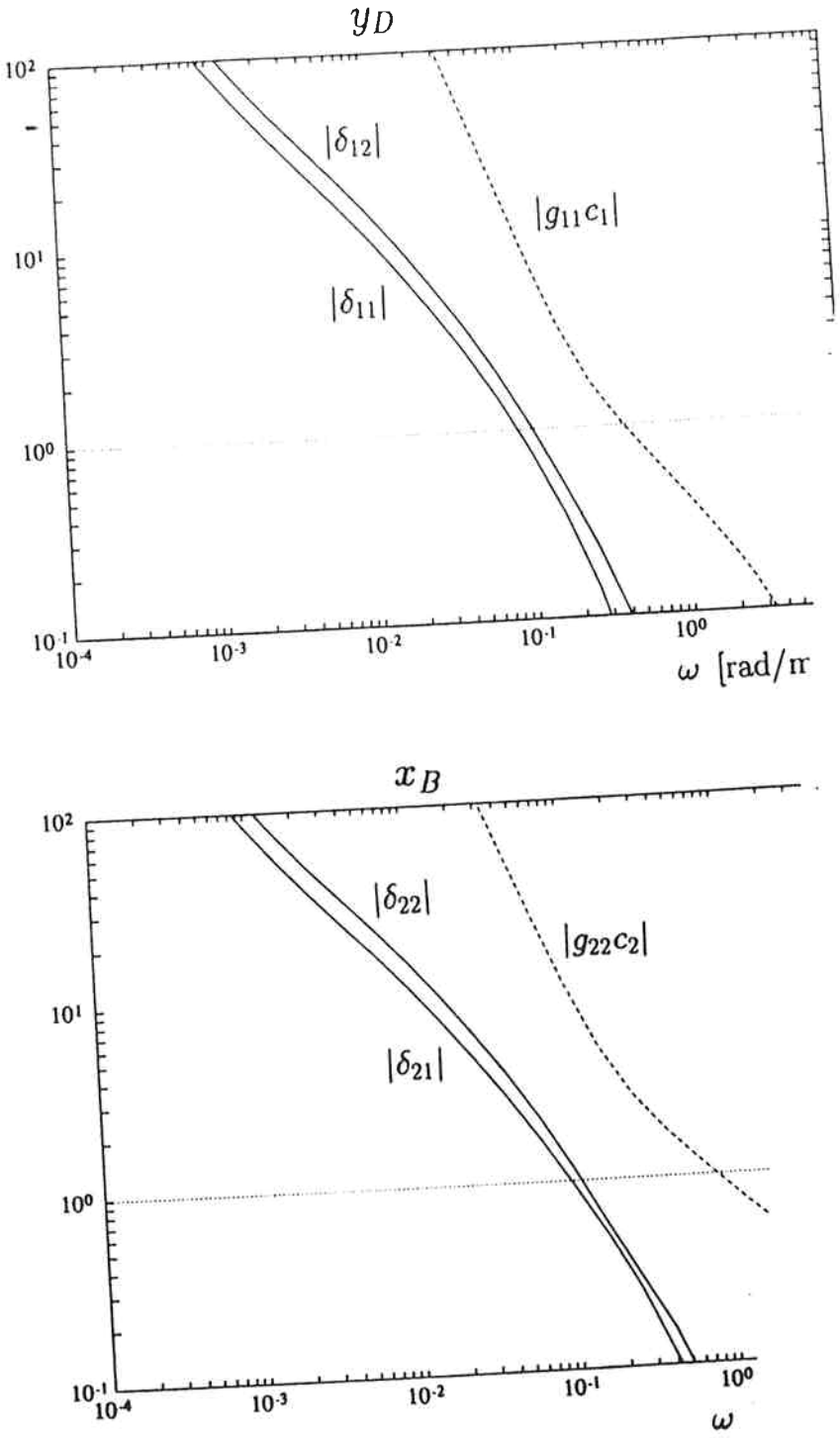

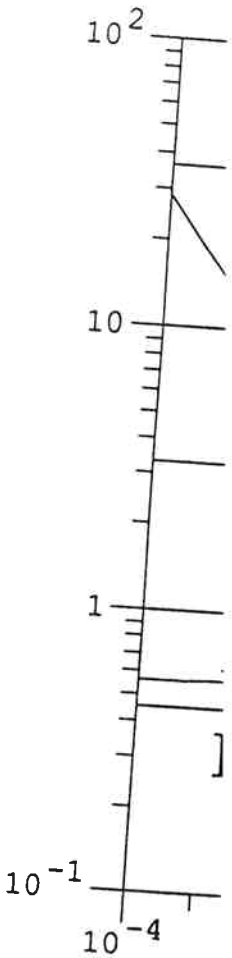

Figur

Figure 9a. Closed loop disturbance gains, $g_{ii}c_i$, for DB configuration.

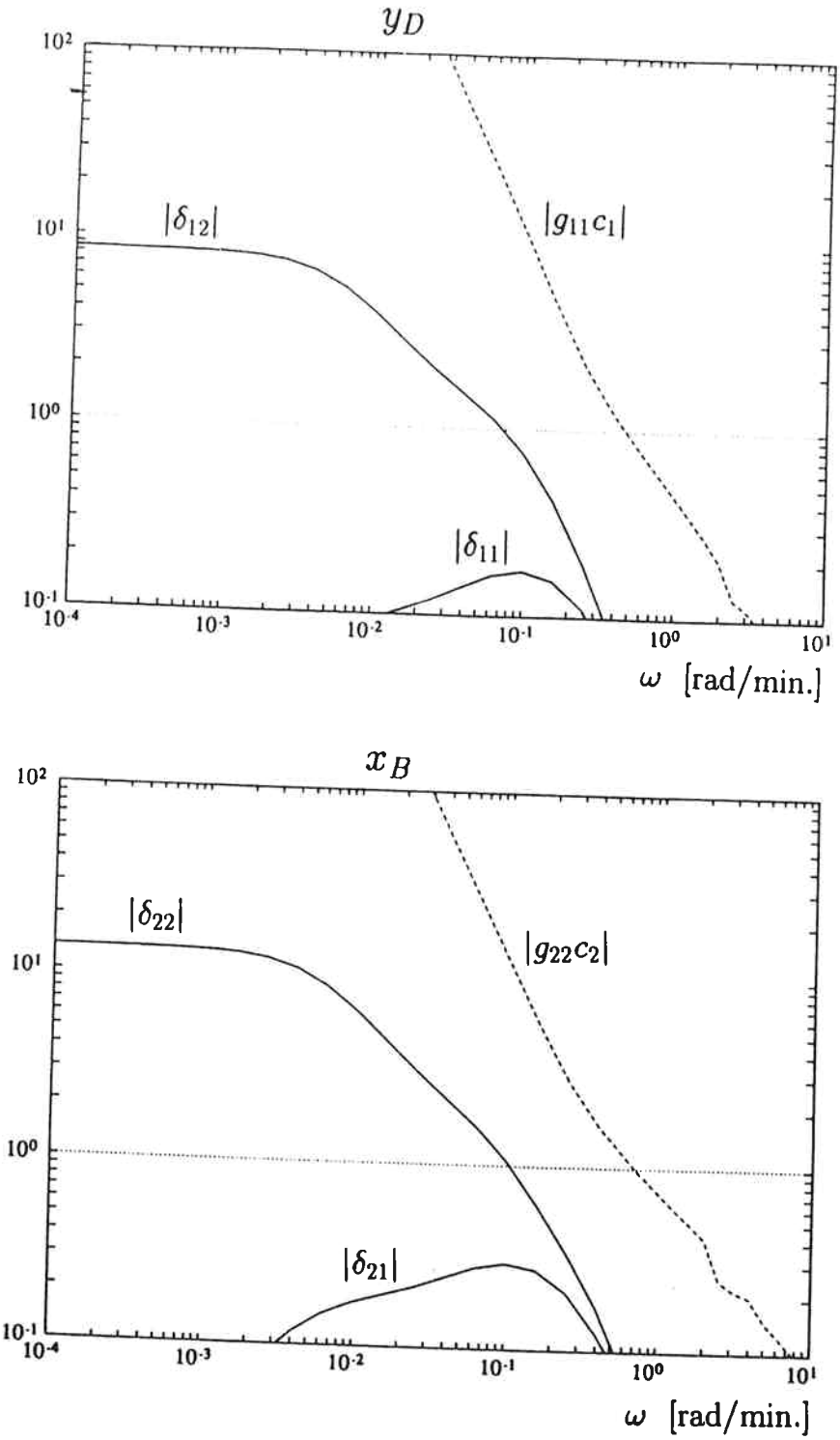

Figure 9b. Closed loop disturbance gains, δ_{ik}, and loop gains, $g_{ii}c_i$, for (L/D)(V/B) configuration.

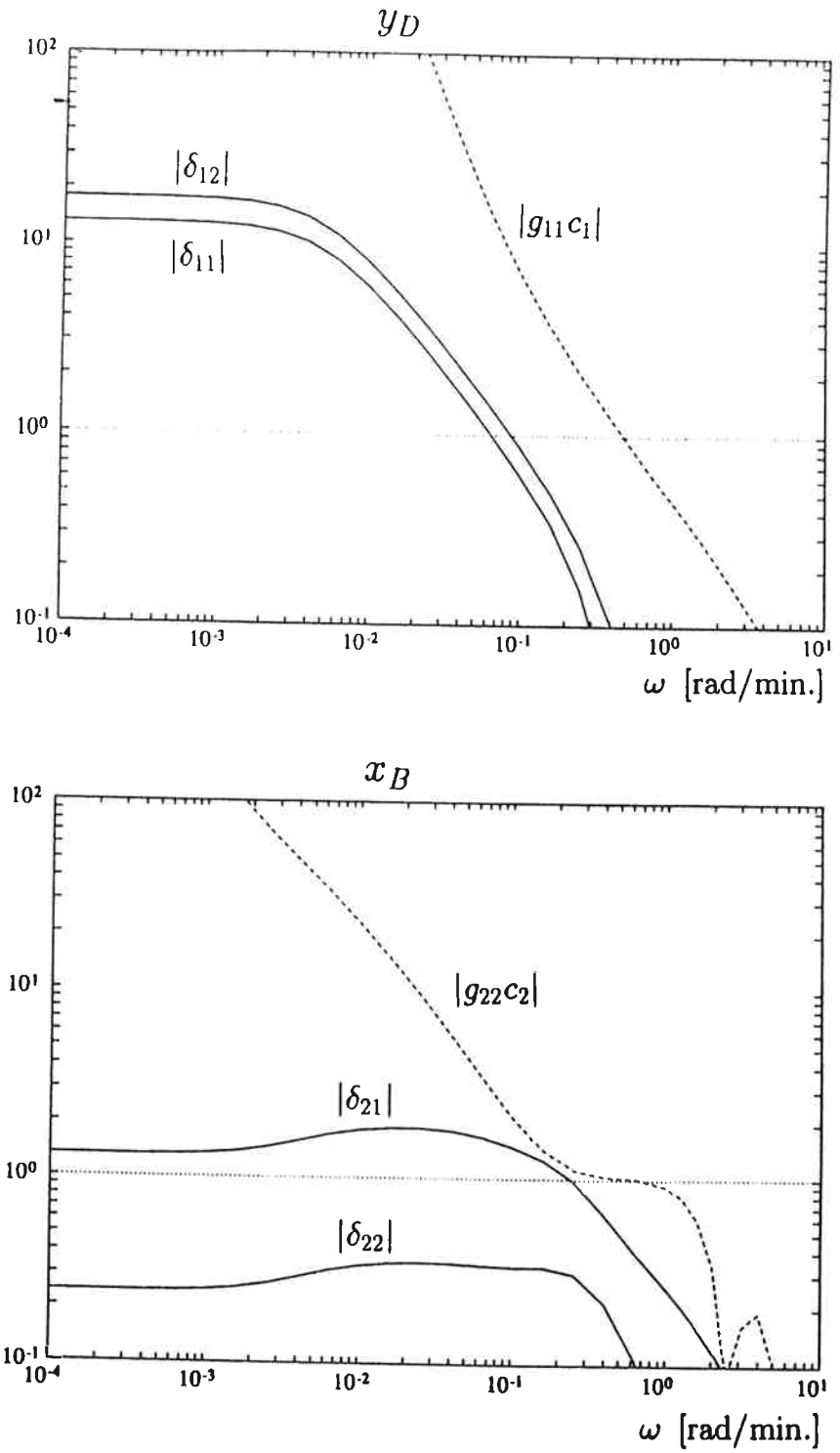

Figure 9c. Closed loop disturbance gains, δ_{ik}, and loop gains, $g_{ii}c_i$, for DV configuration.

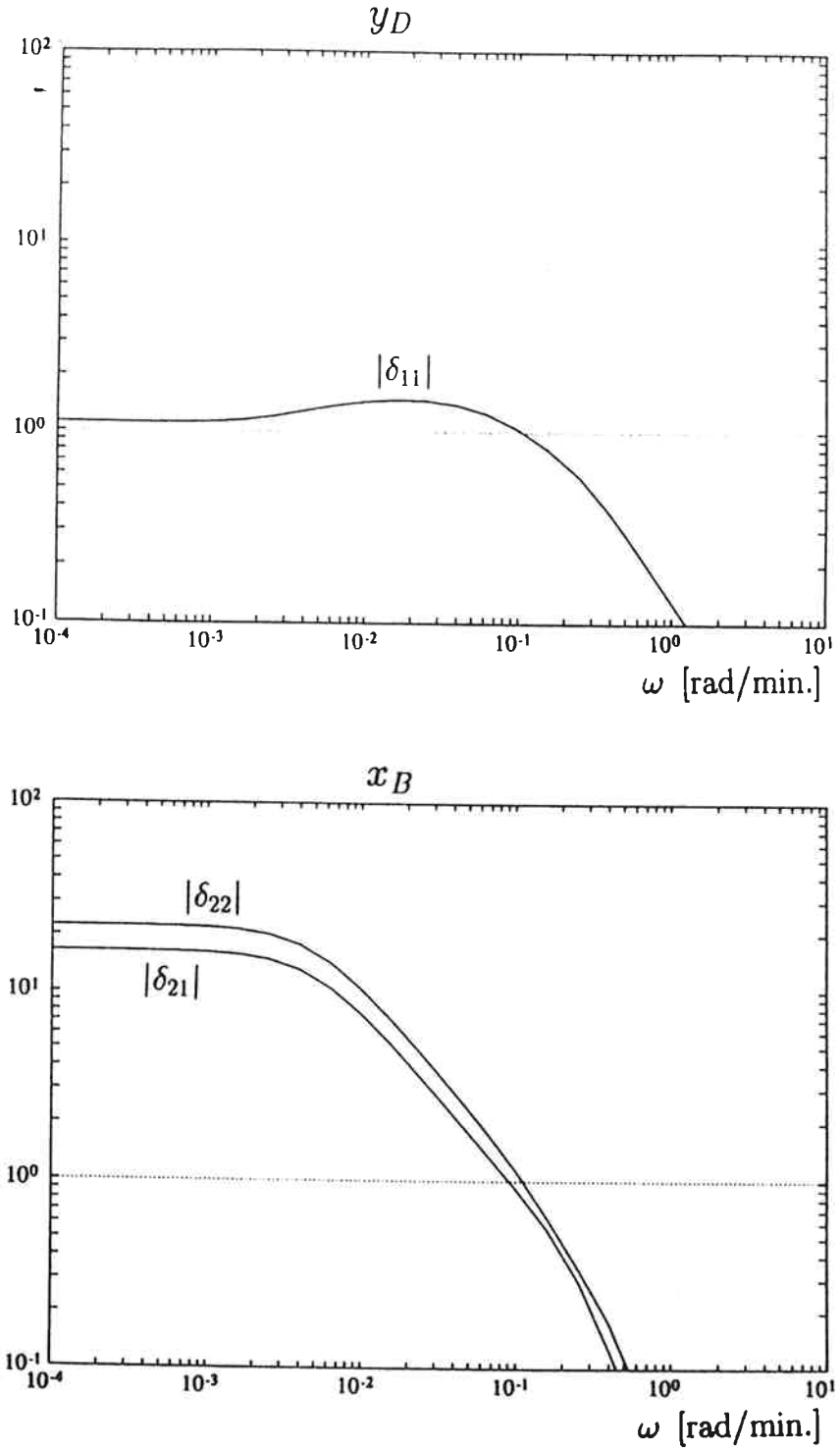

Figure 9d. Closed loop disturbance gains, δ_{ik}, for LB configuration.

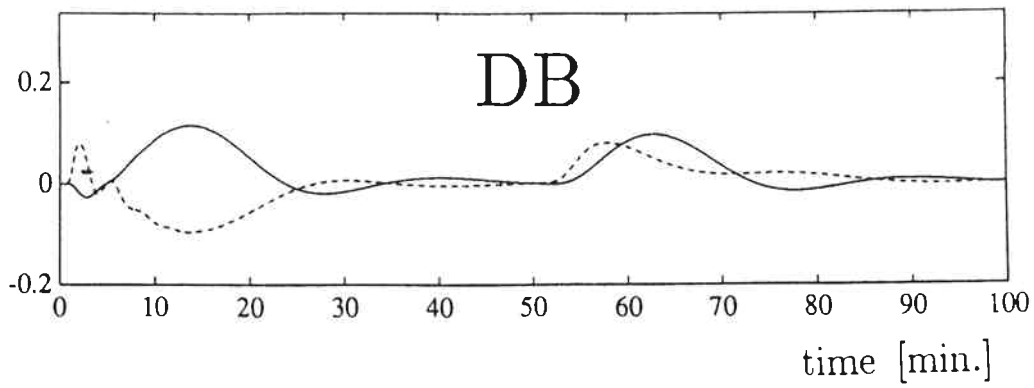

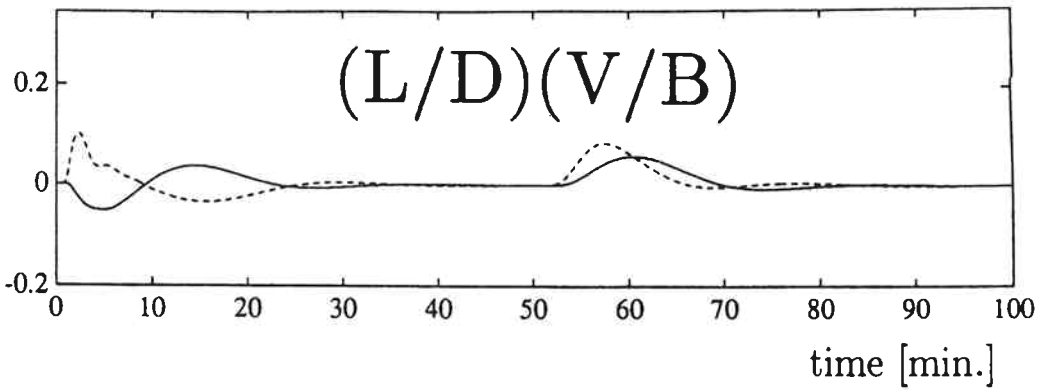

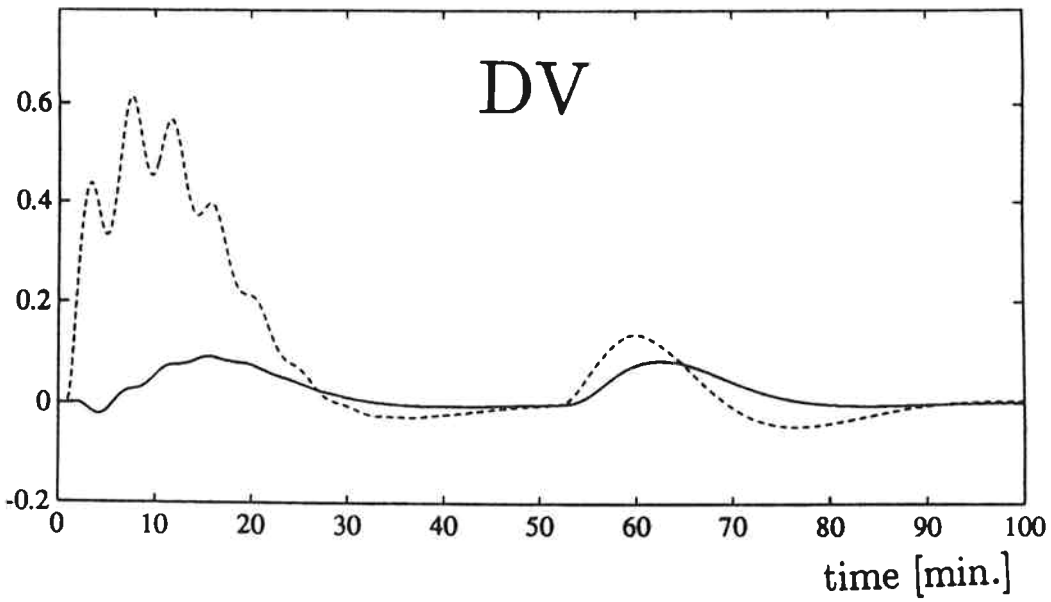

Figure 10. Responses to a 30% increase in F at $t = 0$ and a 20% increase in z_F at $t = 50$min. Solid curve: top composition, y_D. Dashed curve: bottom composition, x_B.

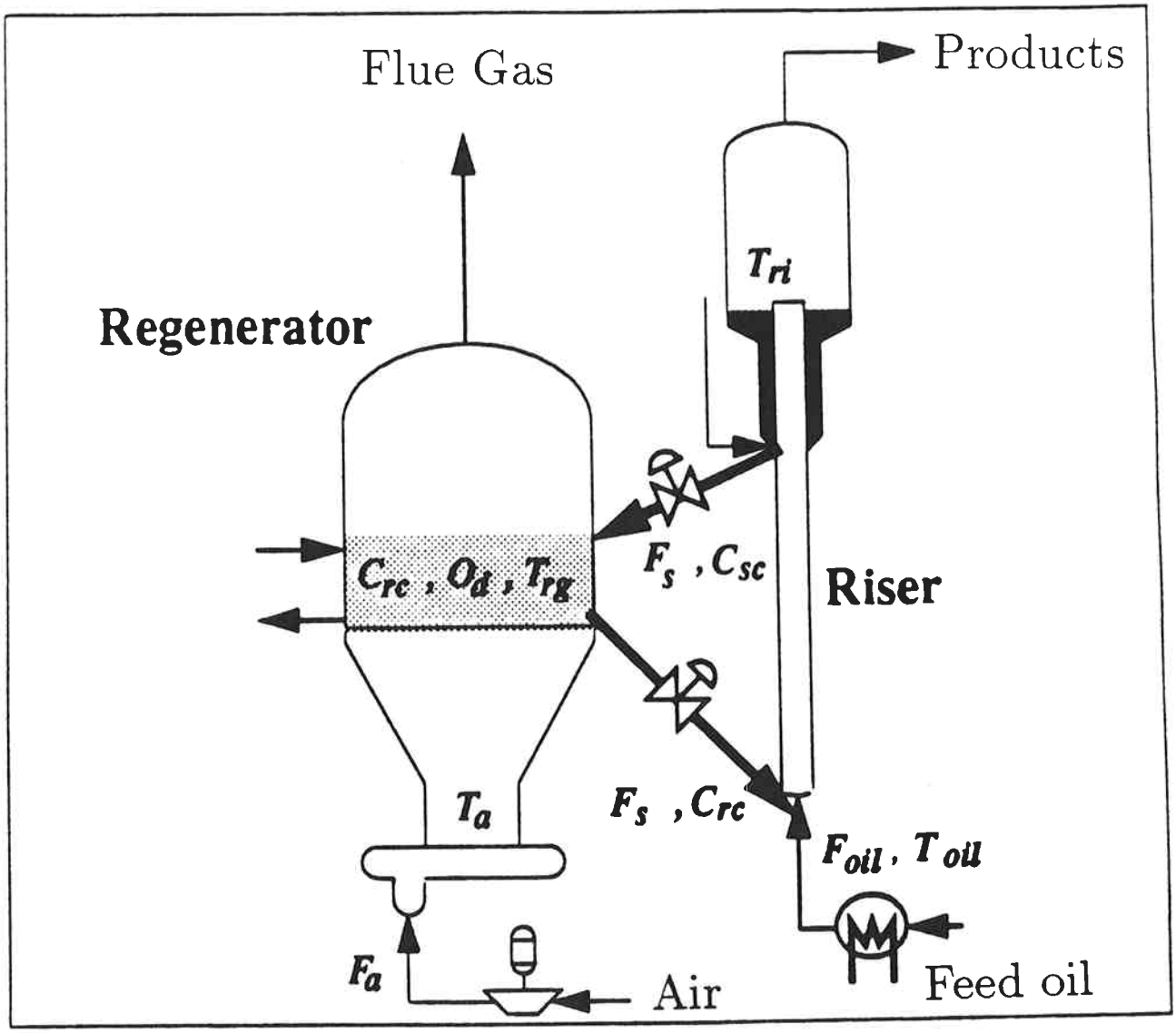

Figure 11 Overview of typical Fluid Catalytic Cracking plant.

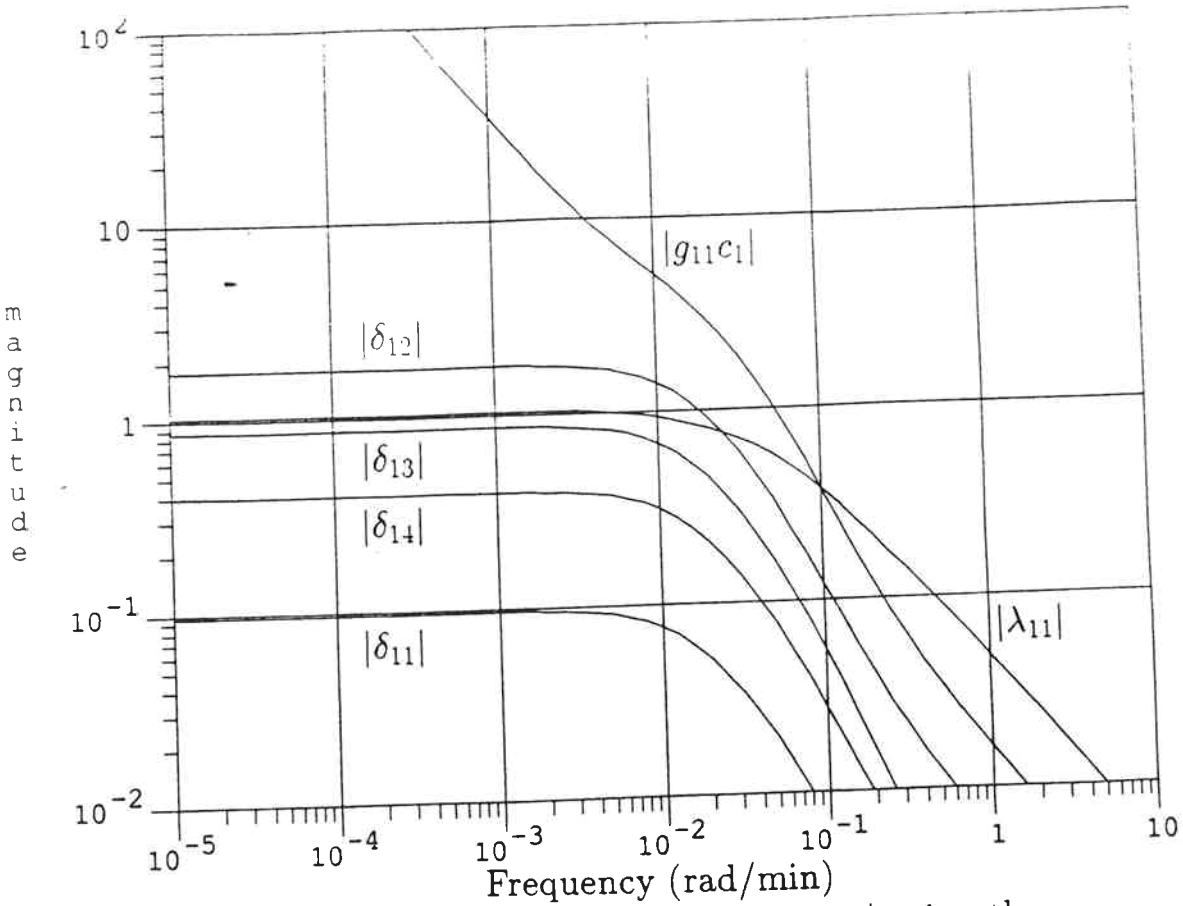

Figure 12a $|\delta_{1k}|$, $|\lambda_{11}|$ and $|g_{11}c_1|$ using the reverse Kurihara structure in example 4

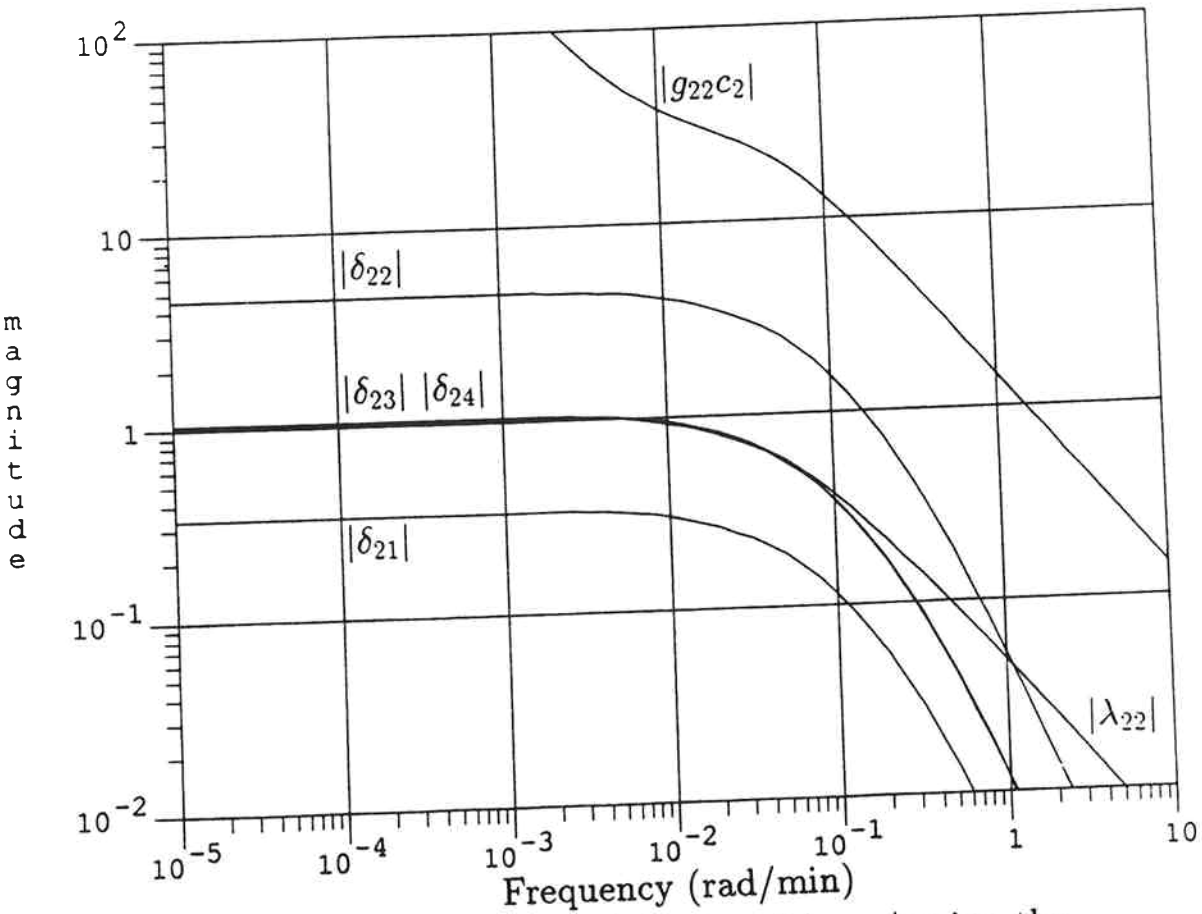

Figure 12b $|\delta_{2k}|$, $|\lambda_{22}|$ and $|g_{22}c_2|$ using the reverse Kurihara structure in example 4

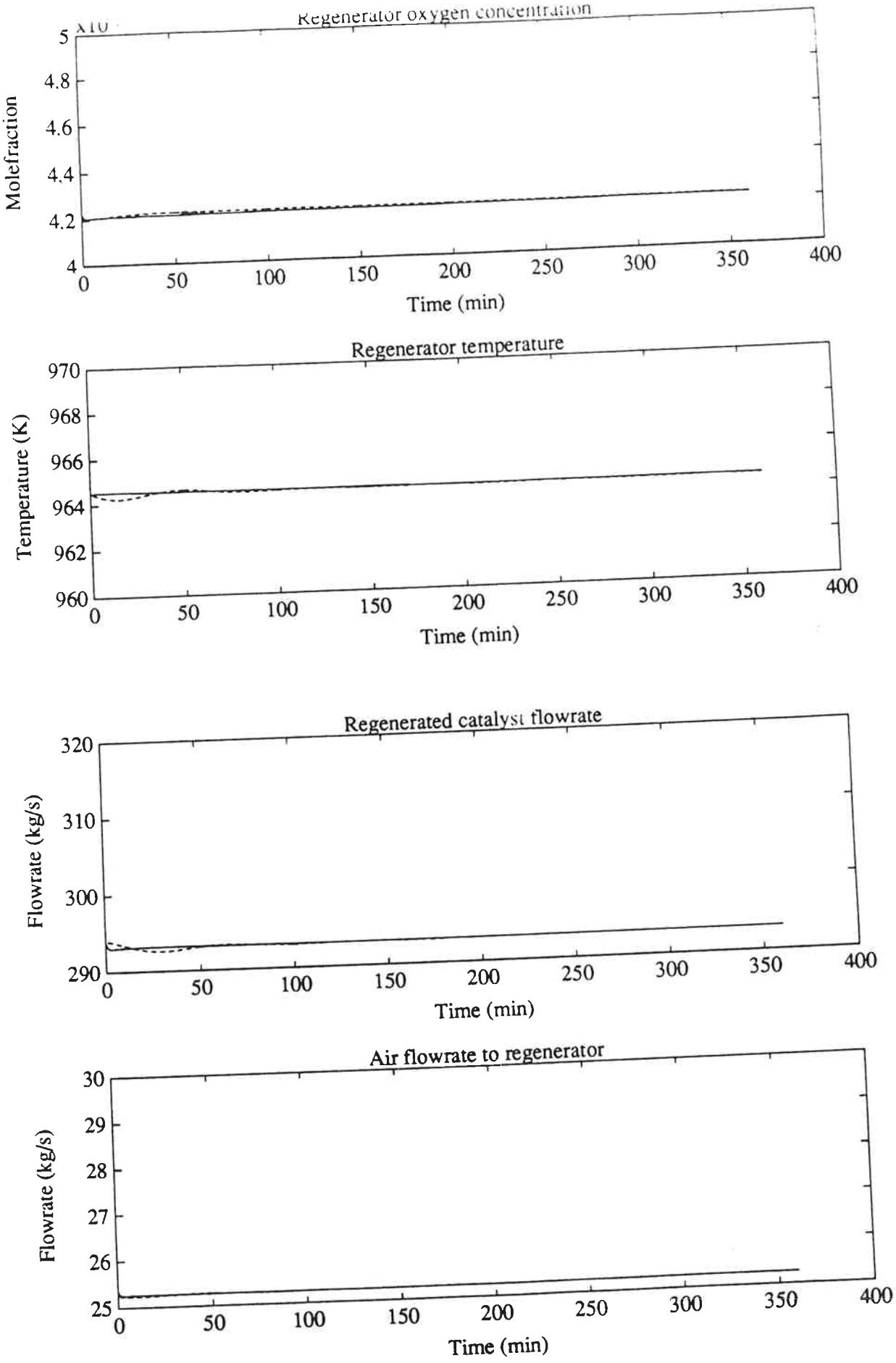

Figure 13 Closed loop response to an increase in the air temperature of 5 K. Solid line: Reverse Kurihara structure. Dashed line: Kurihara structure.

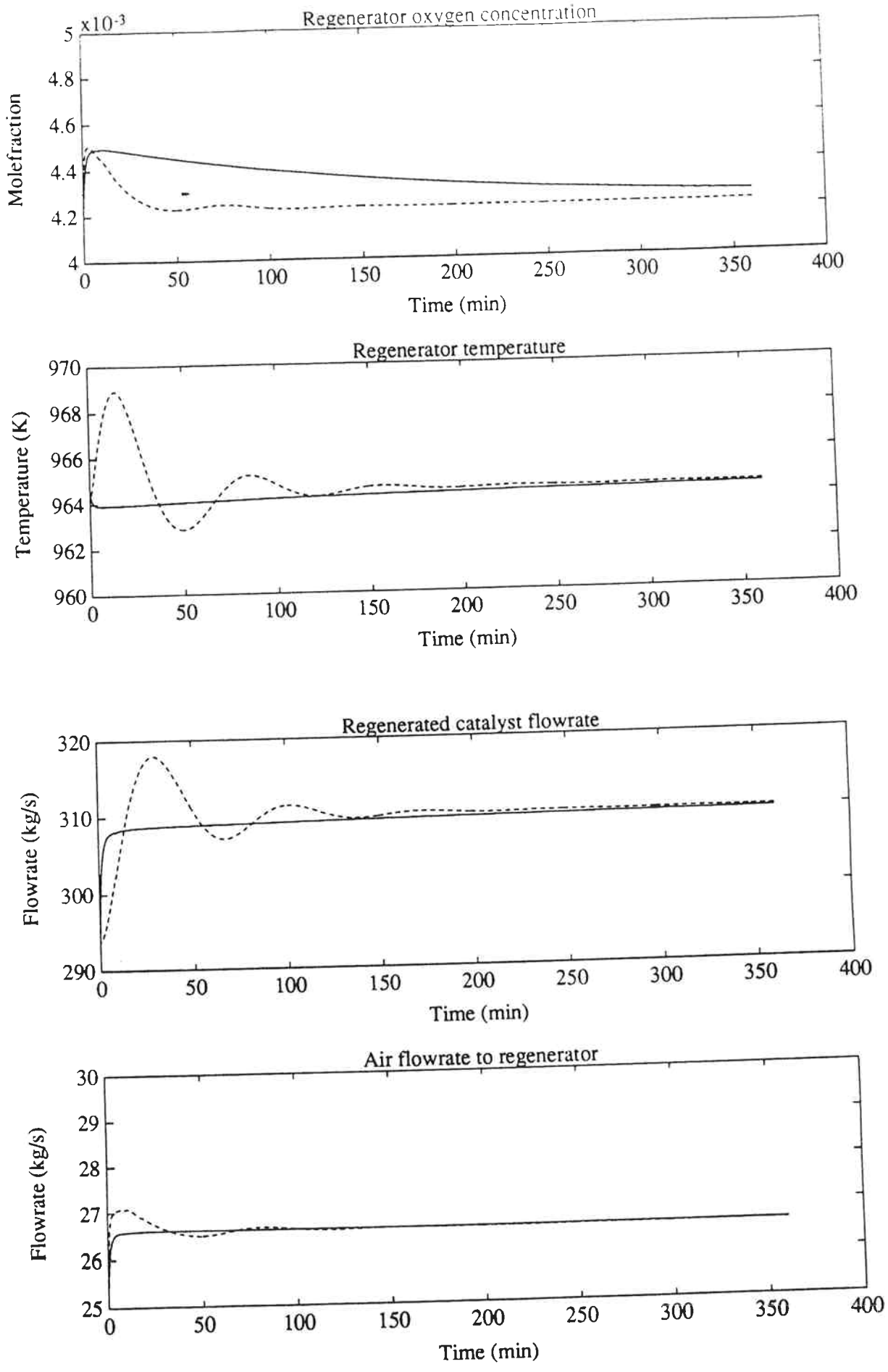

Figure 14 Closed loop response to an increase in the oil flowrate of 2 kg/s. Solid line: Reverse Kurihara structure. Dashed line: Kurihara structure.

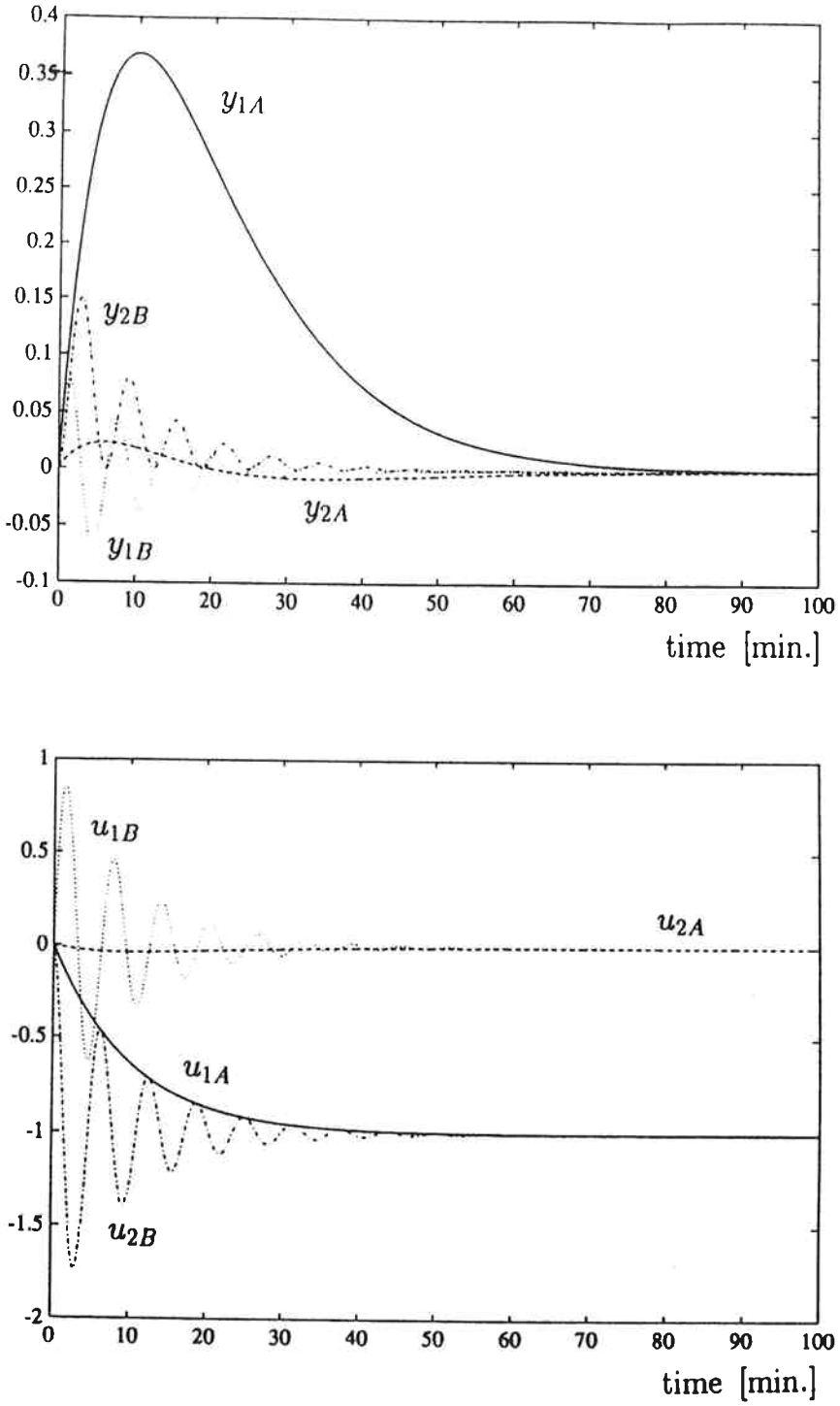

Figure 15. Responses to a unit step disturbance in input 1 for pairing A and input 2 for pairing B. Top: output responses. Bottom: input responses.

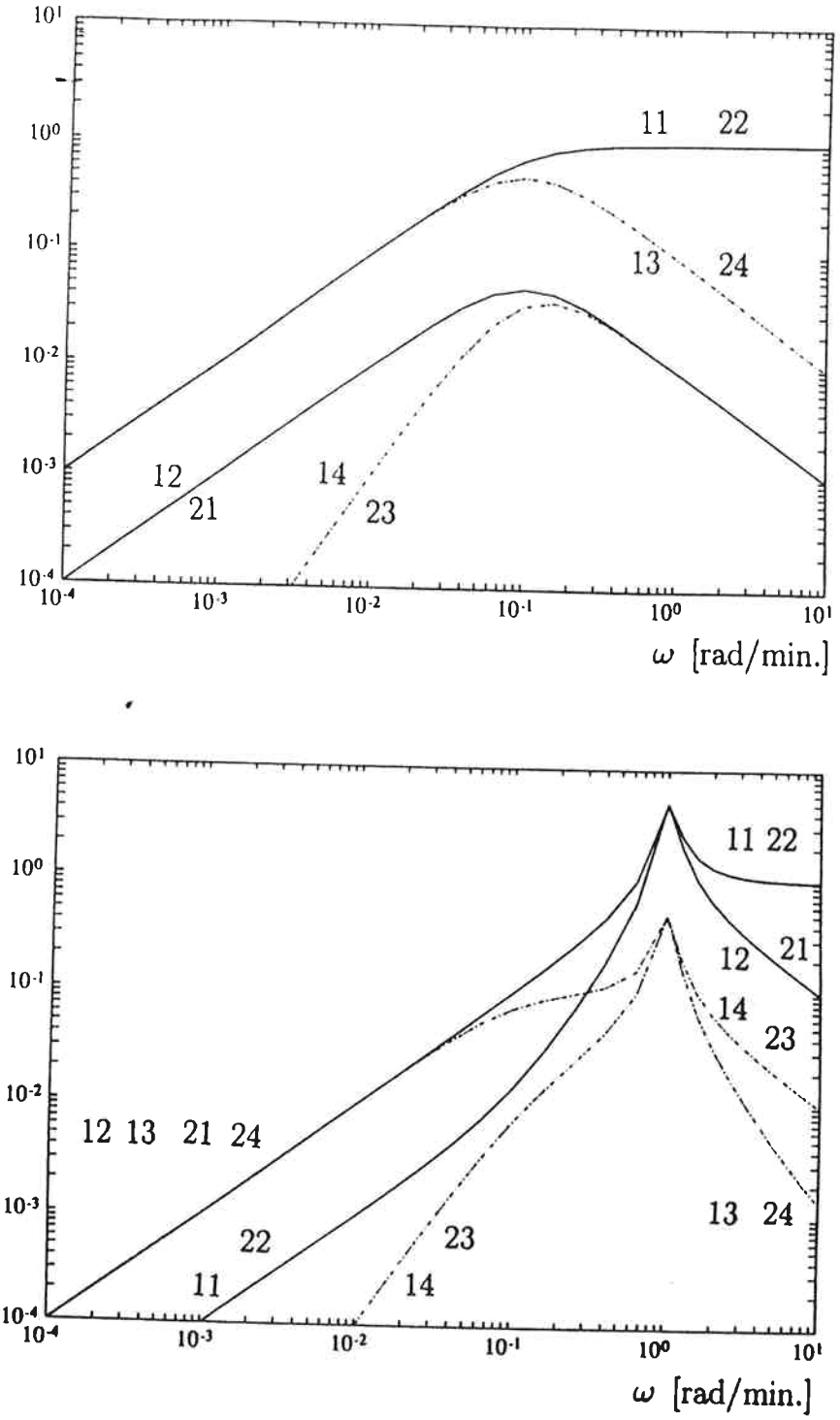

Figure 16. Sensitivity functions for pairing A (top) and pairing B (bottom).